Simultaneous PET-MRI assessment of central α4β2 nAChR availability in participants with obesity compared to normal weight healthy controls under baseline and stimulus conditions

Dissertation
zur Erlangung des akademischen Grades
Dr. med.

an der Medizinischen Fakultät
der Universität Leipzig

eingereicht von:
Tilman Günnewig

Geburtsdatum / Geburtsort:
23.03.1993 / Recklinghausen

angefertigt an / in:
Universität Leipzig / Medizinische Fakultät / Klinik und Poliklinik für Nuklearmedizin

Betreuer:

Prof. Dr. med. Swen Hesse

Dr. rer. med. Michael Rullmann

Beschluss über die Verleihung des Doktorgrades vom: 19.09.2023

2. Table of Contents

3. Abbreviations

β-hCG	β- Human Chorionic Gonadotropin
ACh	Acetylcholine
AChE	Acetylcholinesterase
ARC	Arcuate Nucleus
B_0	Primary Magnetic Field (MRI)
BDI	Beck's Depression Inventory
BF	Basal Forebrain
BFCN	Basal Forebrain Cholinergic Neurons
BBB	Blood-Brain Barrier
BP	Binding Potential
CART	Cocaine- and Amphetamine-Regulated Transcript
ChAT	Choline Acetyltransferase
CHT1	Choline Transporter 1
CNS	Central Nervous System
CT	Computer Tomography
D1R	Dopamine D1 Receptors
D2R	Dopamine D2 Receptors
DA	Dopamine
DB	Diagonal Band
DV	Distribution Volume
DVR	Distribution Volume Ratio
EDE-Q8	Eating Disorder Examination-Questionnaire
fMR Imaging	Functional Magnetic Resonance Imaging
Frontal Cx	Frontal Cortex
GM	Grey Matter
GMP	Good Manufacturing Practice
HD	High Disinhibition
HFD	High-Fat Diet
HPLC	High Performance Liquid Chromatography
HPT	Hypothalamus
ICSS	Intracranial Self-Stimulation
IFB	Integriertes Forschungs- und Behandlungszentrum
LD	Low Disinhibition

LOR	Line of Response
mAChR	Muscarinic Acetylcholine Receptor
MC3/4R	Melanocortin-3/4-receptor
MP-RAGE	Magnetization Prepared Rapid Gradient Echo
MRI	Magnetic Resonance Imaging
MS	Medial Septal Nucleus
MW-U	Mann-Whitney U-Test
NAc	Nucleus Accumbens
nAChR	Nicotinic Acetylcholine Receptor
NBM	Nucleus Basalis of Meynert
Nc. Caud.	Caudate Nucleus
NW	Normal Weight Participants
OB	Participants with Obesity
p.i.	Post Injection
PET	Positron Emission Tomography
PET/MR imaging	Positron Emission Tomography / Magnetic Resonance Imaging
PFC	Prefrontal Cortex
POMC	Proopiomelanocortin
PVE	Partial Volume Effect
SAZ-A	Sazetidine-A
SAT	Sustained Attention Task
SPECT	Single Photon Emission Computed Tomography
TAC	Time-Activity Curves
UTE	Ultra Short Echotime
V/Au Ctx	Visual / Auditive Cortex
VAS	Visual Analogue Scale
VMH	Ventromedial Hypothalamus
VOI	Volume of Interest
V_T	Total Distribution Volume
VTA	Ventral Tegmental Area
VAChT	Vesicular Acetylcholine Transporter
WHO	World Health Organization

List of Figures

List of Tables

4. Introduction

4.1 Obesity and the central cholinergic system

Obesity is a multifactorial syndrome with serious medical sequelae and comorbidities, such as cardiovascular disease, cancer or metabolic syndrome, which poses major challenges for health care systems world-wide.[1] According to the World Health Organization (WHO) and the Global Burden of Disease Study more than 600 million adults worldwide are considered obese[2] underlining today's relevance in firmly approaching this health threat. Several factors have vast impact on obesity's etiology such as socioeconomic status, genetics, environmental circumstances and lack of physical activity combined with modern day diets, which consist of processed foods with high proportions of sugar and saturated fatty acids.[3,4] Currently, surgical treatments such as sleeve gastrectomy are the most effective intervention for sustained weight loss but these procedures are associated with morbidity and mortality.[5] Therefore the search for non-invasive treatment strategies as alternatives to surgical approaches to achieve sustainable weight loss represents a keystone in human obesity research. To identify putative pharmacological interventions, knowledge of the biological factors underlying obesity is essential. The precise role of neurotransmitter circuits involved in the regulation of eating behavior and obesity, however, still needs to be fully explored.

A well-known and highly interesting observation is that the cessation of smoking often leads to weight gain. Rupprecht et al.[6] highlight that smoking cessation leads to an average increase of 10 pounds body weight within the first year. In general, increasing body weight is described to be greatest within first six months of smoking cessation due to decreased metabolic rate and enhanced food intake (Figure 1).[7] McGovern et al. describe the enhanced food intake as "substitutable reinforcers" to compensate for the lack of reward through smoking as the source of substantial weight gain.[7]

Moderate smokers often have a lower BMI than non-smokers, but heavy, more frequent smokers often suffer from obesity as they seem to experience a reduced feeling of reward from smoking as well as from the ingestion of palatable food items.[6,8] In another study, Kovacs et al. showed that young adult female smokers with the tendency to disinhibited eating behavior after being presented a food prime, would smoke more to compensate for their food craving.[9]
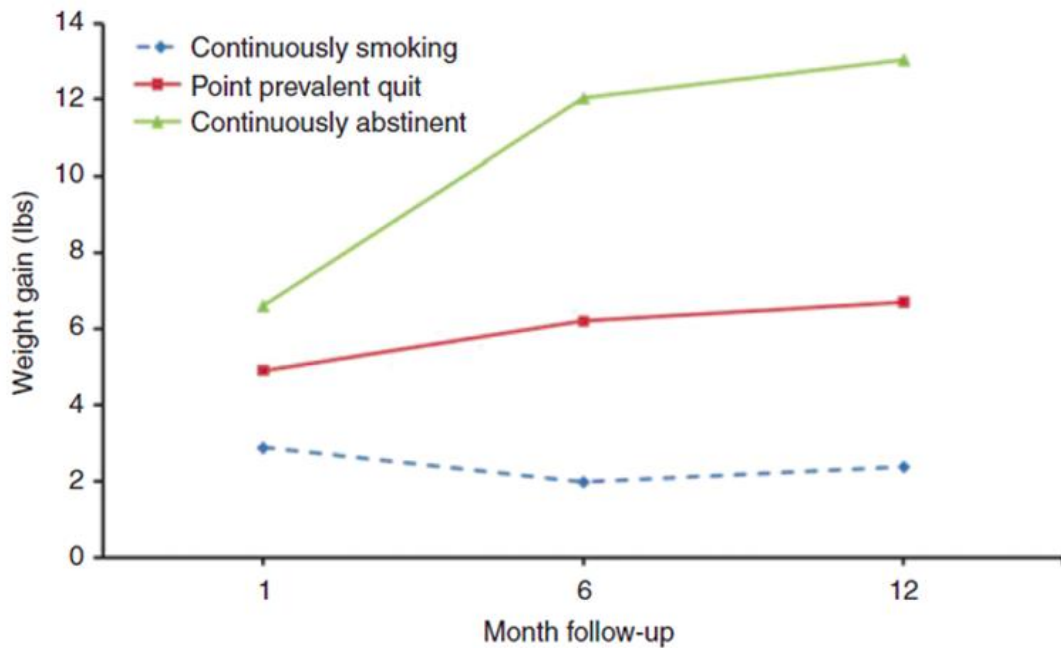
Figure 1*: Association Between Smoking Cessation and Weight Gain*

Increase of body weight is highest with continuous smoking cessation

On a behavioral level, individuals with obesity seem to have a tendency to immediately rewarding values or actions, irrespective of potential long-term negative outcomes.[10] Furthermore, a great susceptibility to environmental food cues leading to habitual actions of eating in a stimulus-response paradigm points out to impairments in behavioral choice and alterations in traits of impulsivity.[10] As such, individuals with obesity share neurobiological mechanisms similar to individuals that suffer from addiction.[11] This includes alterations of dopaminergic mesolimbic reward signaling as well as dysfunctional pathways of neuromodulation involved in the evaluation and value attribution of external stimuli. Understanding altered salience processing in obesity is therefore pivotal.

Interestingly, the particular computation of attentional as well as reward signaling involves cholinergic neuromodulation, through expression of nicotinic acetylcholine receptors (nAChRs).[12,13] In rats, nicotinic stimulation increased the tendency to choose immediate yet smaller rewards in comparison to greater reinforcers.[14] Preclinical findings in mice suggest that high-fat diets increase exploratory behavior and the density of nAChRs subtypes in brain areas like prefrontal cortex (PFC) or midbrain, which are associated with the regulation of impulsive behavior.[15] This highlights the

potential involvement of cholinergic signaling in behavioral aspects of impulsive character traits affecting feeding behavior.

However, studies that investigate task-related cholinergic signaling in a baseline versus stimulus design in human obesity do not exist. To explore the relationship between cholinergic network modulation and its implications on eating behavior, this study will elucidate structural and functional characteristics of the α4β2 nAChR in human obesity.

4.2 Cholinergic Neurotransmission

Neurotransmitters are chemicals that allow inter-neuronal communication throughout the body. There are a number of excitatory and inhibitory neurotransmitters used for different functions, including acetylcholine (ACh), glutamate, GABA, glycine, dopamine, norepinephrine, and serotonin.[16] They coordinate brain activity at a molecular level and therefore regulate, e.g. emotional states, homeostasis, cognition and behavior.[17] Imbalance of neurotransmitter homeostasis and therefore neuronal circuits can lead to several psychiatric disorders, such as schizophrenia[18], depression[19] or neurodegenerative diseases, such as Alzheimer's[20] or Parkinson's disease.[21] Alterations in neurotransmitter signaling also maintain addiction[22] and contribute to altered eating behavior.[23] Physiologically, neuronal signaling transmitted by ACh, which can also be referred to as cholinergic signaling, mediates pivotal cognitive processes[24] such as the generation of attention[25], working memory[26] or informational processing of salient cues[27], but it also has a central role in mesolimbic reward signaling.[28]

There are two types of cholinergic receptors: the metabotropic, G-protein coupled muscarinic AChR (mAChR) and the cationic, nicotinic AChR (nAChR), each with individual functions in e.g. cognitive processing.[26] In the latter, both nicotine as well as ACh function as receptor agonists. ACh is synthesized by the enzyme choline acetyltransferase (ChAT). When an action potential arrives at the presynaptic neuron, neurotransmitters are released into the synaptic cleft by a presynaptic Ca^{2+} influx and the consecutive process called exocytosis. ACh binds as a ligand to the corresponding receptor situated at the postsynaptic neuron and either induces an influx of cations through a conformational receptor change (nAChR) or metabotropic, G-protein

coupled signaling cascade (mAChR). These processes in turn generate an action potential at the postsynaptic neuron and thus neuronal signaling is conveyed. When ACh is released from the postsynaptic receptor, it gets hydrolyzed by the enzyme acetylcholinesterase (AChE) into choline and acetate. Then, both molecules are transported back into the presynaptic neuron by the high-affinity choline transporter (CHT1)[20] (Figure 2).
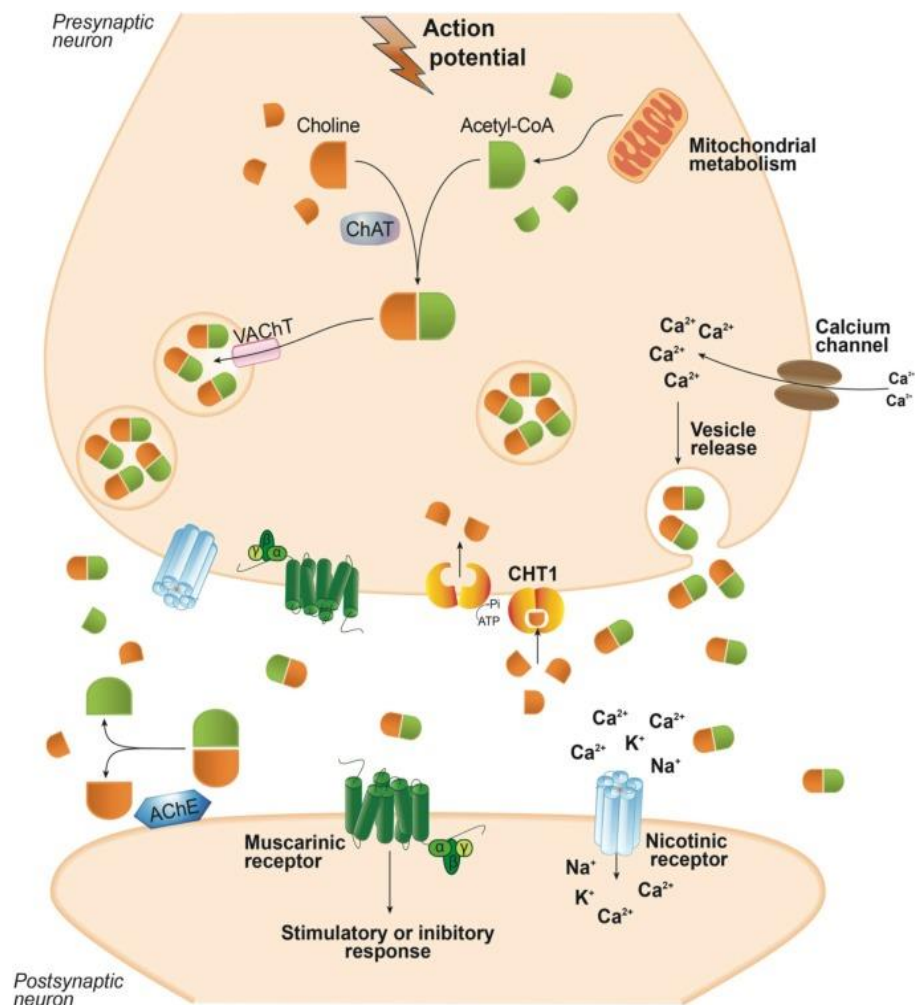
Figure 2: Cholinergic Neurotransmission

Abbreviations: CHT1 – Choline Transporter 1; VAChT – Vesicular Acetylcholine Transporter; ChaT – Choline Acetyltransferase; AChE – Acetylcholinesterase

4.3 Structure and Receptor Kinetics of nAChR

The nAChR are ligand-gated cation channels consisting of nine α- (α2 to α10) and three β-subunits (β2-β4).[29] The nAChRs comprise five cylindrical, transmembrane subunits, arranged in heteromeric αβ-combinations (e.g. α3β4* containing nAChRs; the asterisk refers to one or more additional subunits that could be associated with the receptor), homomeric nAChRs (α7–α9) and a heteromeric α-combination (α9 with α10), all adding to a broad nAChR landscape (Figure 3).[30] The accessory subunits influence the receptor characteristics, in terms of pharmacological and biophysical properties, as well as their response to allosteric modulation.[29] Different nAChRs with different amino acid sequences therefore react in a different manner to their ligand, each with distinct affinity, sensitization and cation permeability profiles.[31] The α4β2 nAChR is the most abundant in the mammalian brain, with the highest receptor density in the thalamus, followed by a rather intermediate density in cortical and caudate regions and finally lowest density in white matter.[32,33]
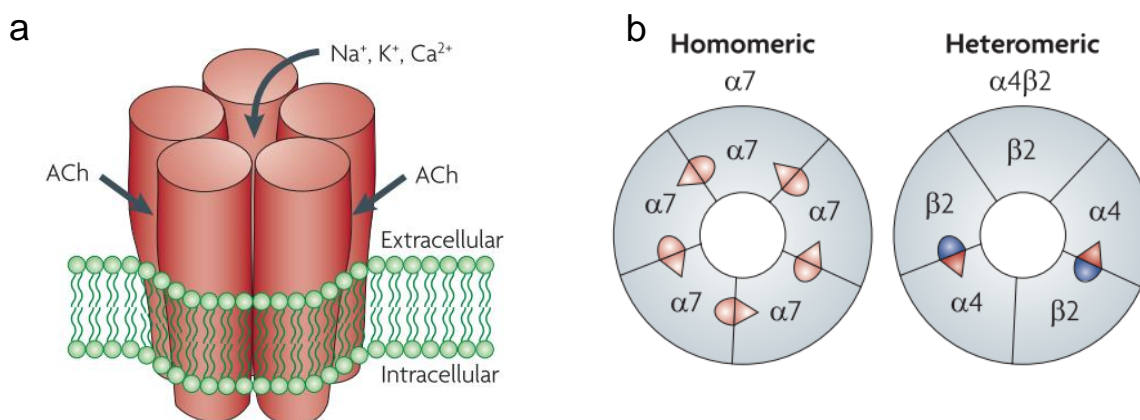
Figure 3: Structure of nAChR

a – depicts the five transmembrane subunits with non-selective cation channels and two ACh binding-sites

b – examining the distribution of nAChR in the brain, one can find two most common types: the α7* homo-oligomer, characterized by a fast activation, a low affinity for ACh, and a high Ca^{2+} permeability, and the α4β2 hetero-oligomer, typified by a high agonist affinity and slow desensitization and lower Ca^{2+} conductance[34]

Graupner et al.[28] describe that the nAChR can be subdivided in four different functional states (Figure 4), according to e.g. abundance of receptor ligand and shifting timeframe from activated, desensitized state to resting state and thus being ready for receptor-ligand-interaction (Figure 4). They compile the four states to "the resting (closed) state (R), the open state (O), the fast-onset desensitized (closed) state (I), and the slow-onset desensitized (closed) state (D)[…]." Desensitization occurs after ligand binding and receptor activation. Although, ligand affinity is highest in the desensitized nAChR state compared to the activated one, the nAChR can only exert its excitatory function in the O state.[28,35]
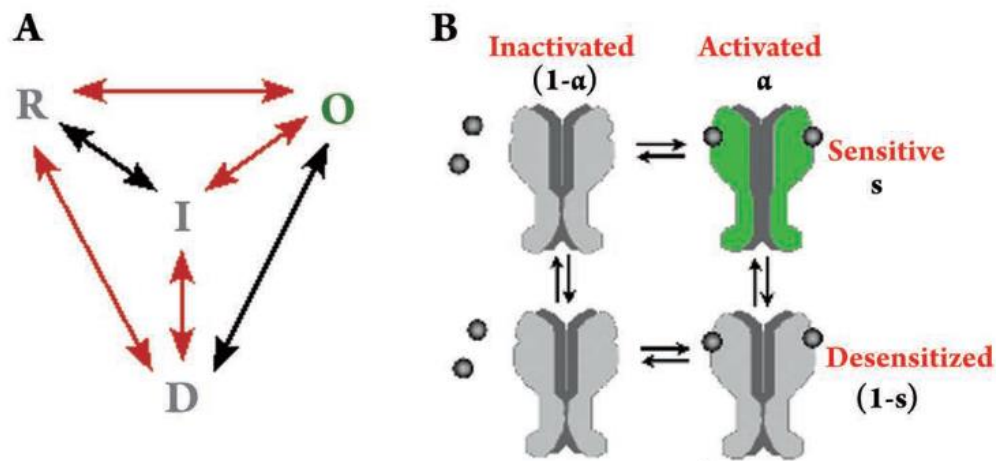
Figure 4: Essential nAChR Kinetics

A – Red arrows indicating more common kinetics in regards of nAChR conformational changes

B – Depiction of all four conformational receptor states, according to prior receptor binding and allosteric modulation

Research in smokers showed that chronic tobacco smoking leads to a nicotine-induced upregulation of nAChR[36] as well as profound changes in conformational states. This results in desensitized nAChR disrupting endogenous ACh signaling, which is pivotal for computing environmental salient cues, e.g. visual food stimuli. Yet, studies that examine similar alterations in cholinergic signaling in human obesity and how this potentially affects eating behavior do not exist.

4.4 Topography of central nAChR

There are three main cholinergic projection points innervating numerous areas in our central nervous system (CNS): First, nuclei in the basal forebrain: namely the medial septal nucleus (MS), the nucleus basalis of Meynert (NBM) and the diagonal band (DB). These nuclei project to the hippocampus, most cortical regions as well as some subcortical nuclei. Second, the pedunculopontine-lateral dorsal tegmental nuclei from the brainstem, innervating the thalamus, midbrain and other regions in the brainstem and at last, striatal interneurons (Figure 5).[37]
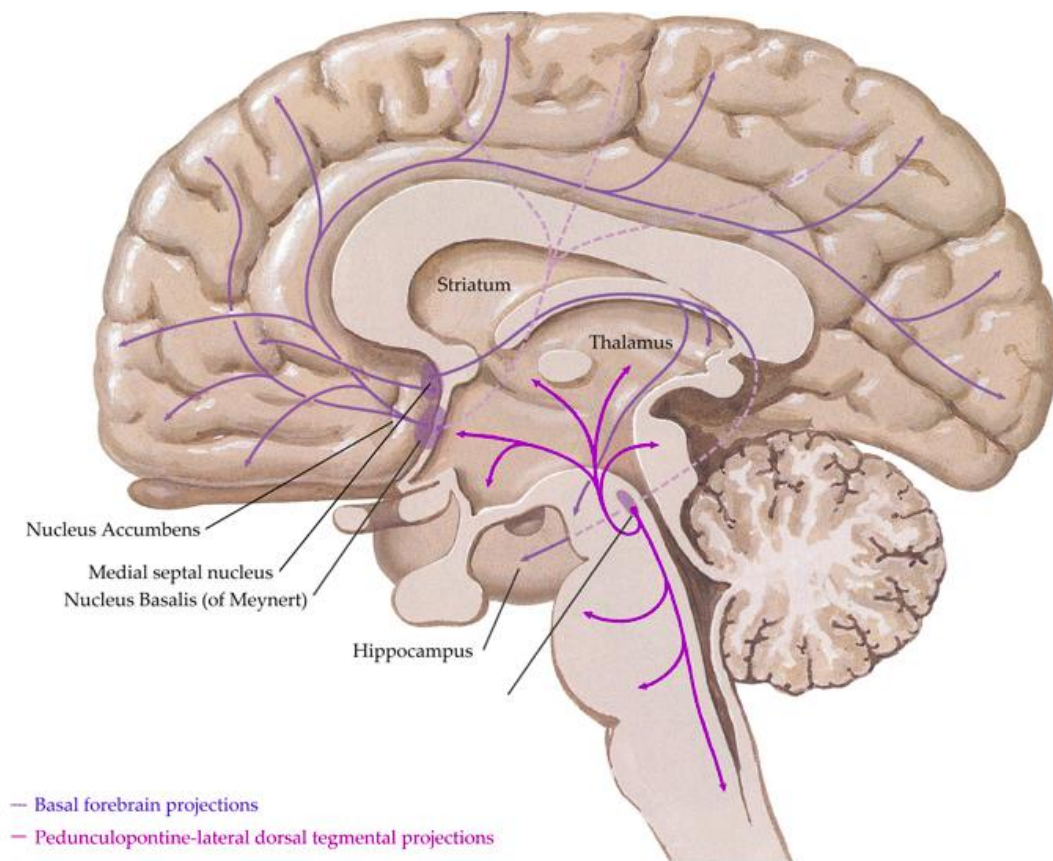
Figure 5: Central Cholinergic Projection Points

Table 1 gives an overview of distinct cholinergic topography. Here, cholinergic cell group Ch4 is especially notable, as the Nucleus basalis of Meynert (NBM) projects to almost the entire neocortex.[26]

Table 1: Central Cholinergic Projection Points

System	Cholinergic cell group	Containing nuclei	Target
Basal forebrain	Ch1	Medial septum	Hippocampus
Basal forebrain	Ch2	Vertical limb of the diagonal band of Broca	Hippocampus
Basal forebrain	Ch3	Lateral part of horizontal limb of the diagonal band of Broca	Olfactory bulb
Basal forebrain	Ch4	Nucleus basalis magnocellularis (i.e., nucleus basalis of Meynert), Globus pallidus, neurons lateral to the vertical limb, and neurons in the medial part of the horizontal limb of the diagonal band of Broca	Neocortex, Basolateral amygdala
Brainstem	Ch5	Pedunculopontinus, cuneiform, parabrachial area	Thalamus, Basal ganglia
Brainstem	Ch6	Lateral tegmental nucleus	Thalamus, Basal ganglia

4.5 Cholinergic Neuromodulation

Picciotto et al.[38] define neuromodulation "as a change in the state of a neuron, or group of neurons, that alters its response to subsequent stimulation". Neuromodulators alter neuronal excitability in the brain and thus change the state of neuronal networks and their response to new salient stimuli from a constantly changing environment. ACh acts as a neuromodulator on a broad spectrum of pre-, peri- and postsynaptic neurons, *en passant* synapses, as well as point-to-point synapses, enabling it to modulate various neurons of different neurotransmitter systems (Figure 6).[24] This leads to distinct neuromodulation processes: balancing out neuronal excitation, nAChRs can decrease neuronal excitation of high excitatory circuits. Nonetheless, it can also enhance neuronal excitation of low excitatory circuits.[39] Stimulation of nAChR also induces the release of other neurotransmitters, such as e.g. GABA, glutamate or dopamine[38], enhance synaptic plasticity[40] or even promote encoding in the hippocampus.[41]
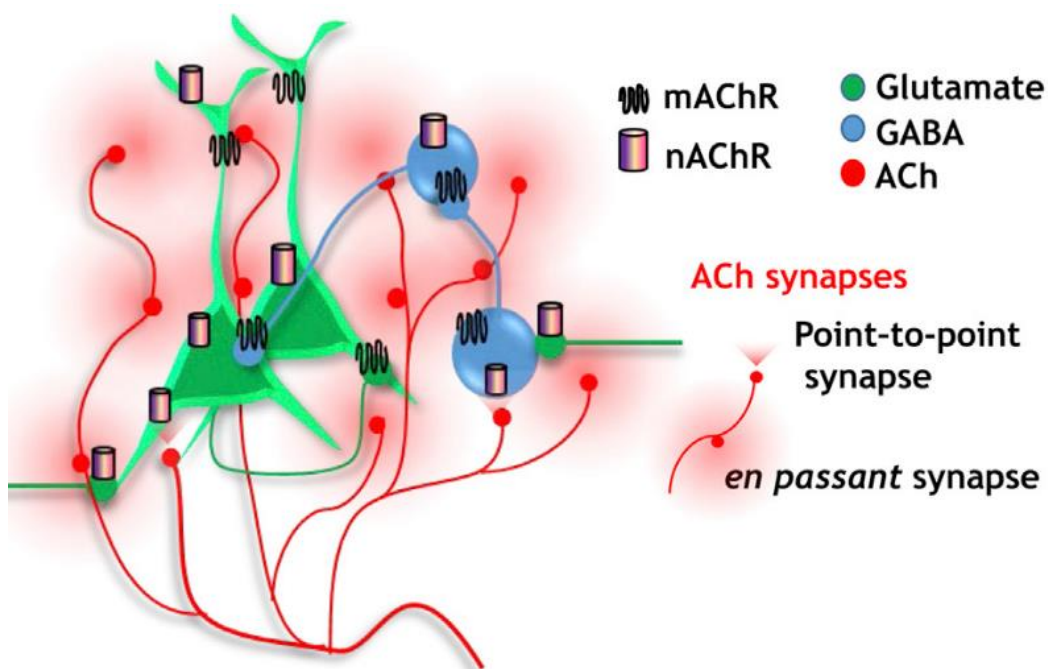
Figure 6: Cholinergic signaling and its interaction with other neuronal groups (such as GABAergic and glutamatergic neurons)

4.5.1 Cholinergic Neuromodulation and Cognitive Processes

The cholinergic system as a pharmacological target is already broadly applied in modern day dementia treatment strategies to improve cognitive performance with cholinesterase inhibitors such as rivastigmine.[42]

Interestingly, one crucial function of cholinergic signaling is the generation of attention and the detection of new salient sensory cues. Sarter et al. define cue detection as "a cognitive process that involves the incorporation of a cue into the ongoing cognitive and behavioral process and therefore allows the cue to control behavior".[27] Due to its unique neuromodulation profile, cholinergic network modulation acts on different time scales: i.e. rather fast, transient (phasic) responses happening within a millisecond timeframe, as well as slower, longer lasting (tonic) modulatory effects.[24,25,38] The phasic release of ACh into the prefrontal cortex (PFC) allows for the detection of the cue, while the longer lasting, tonic increase of ACh release represents a higher neuromodulation tone to enhance attentional performance (Figure 7).[27]

Optogenetic stimulation of cholinergic transients in mice in a stimulus-response paradigm even increases invalid reporting of cues due to artificial dysregulation of phasic cholinergic signaling.[43] Parikh et al.[13] describe the tonic release profile with changes in cholinergic activity that occur over minutes with higher tonic levels predicting greater amplitudes of phasic signals and enhanced cue detection. The tonic release profile therefore represents the classic understanding of cholinergic signaling as "arousal"-promoting. Paolone et al. highlighted improved attentional performance in mice in a sustained attention task (SAT) that had previously performed poorly, after the administration of partial α4β2 nAChR agonist (ABT-089) in contrast to administration of amphetamine showing no improvement in attentional behavior.[44] Also, a substantial increase in extracellular prefrontal cholinergic activity showed a positive correlation with better results in the aforementioned SAT in comparison to mice with lower increase in prefrontal ACh levels.[44]
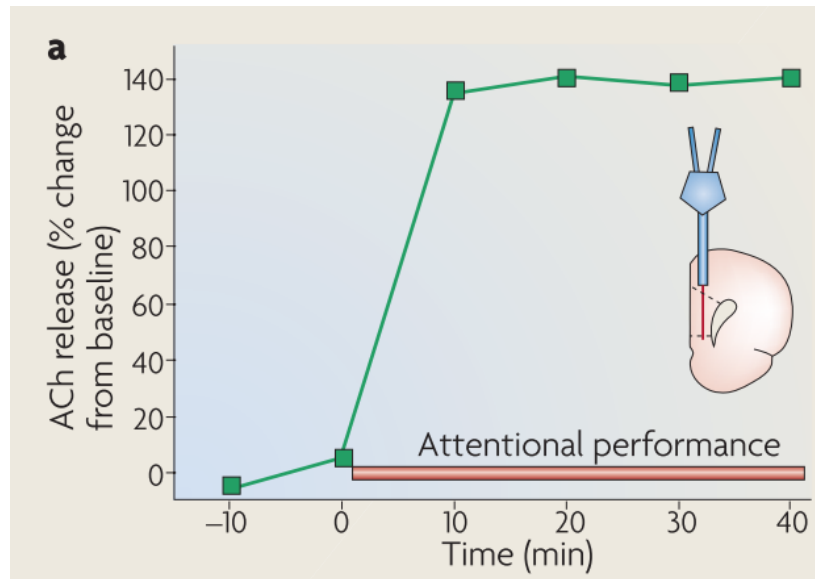
Part a: prefrontal cortex microdialysis data *in vivo* of animals performing an attentional task: Tonic increase of ACh release compared to baseline enhances attentional performance on a scale of a few minutes through activation of thalamocortical circuits, eventually amplifying phasic ACh release.[27]
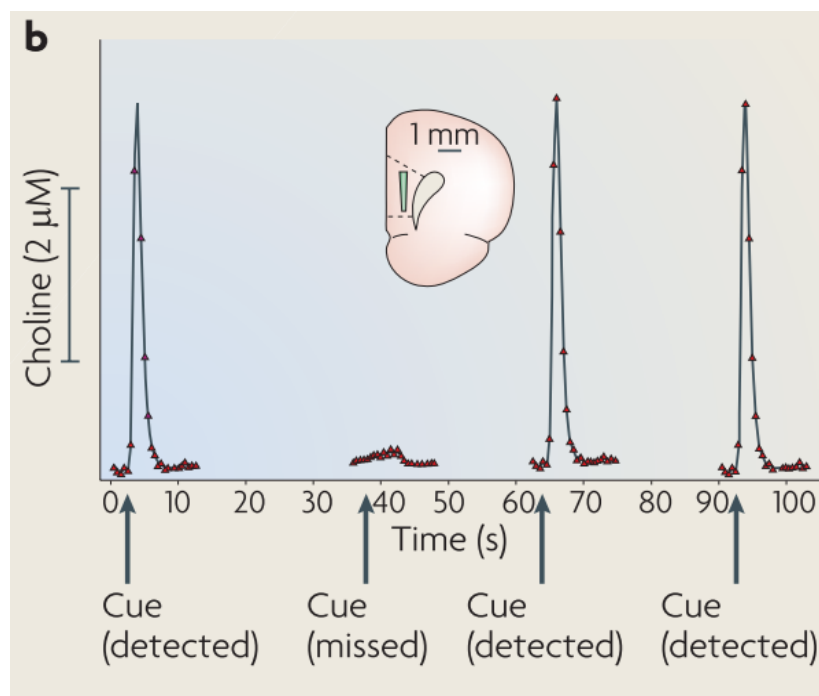
Part b: phasic releases of ACh are essential for the detection of sensory cues.[27]

Figure 7: ACh Release Profiles in Attentional Performance

Adapted by permission from: Nature, Nature Reviews Neuroscience, Phasic acetylcholine release and the volume transmission hypothesis: time to move on, Sarter et al., © 2009

On receptor dynamics level, cholinergic signaling enhances the signal-to-noise ratio, meaning the ability to differentiate between irrelevant and relevant sensory input, of new afferent information through distinct processes (Figure 8): through stimulation of nAChR it enhances afferent thalamocortical signaling, whereas it decreases cortical excitatory feedback connections and internal processing, as these processes would interfere with upcoming new information about environmental stimuli.[45,46]
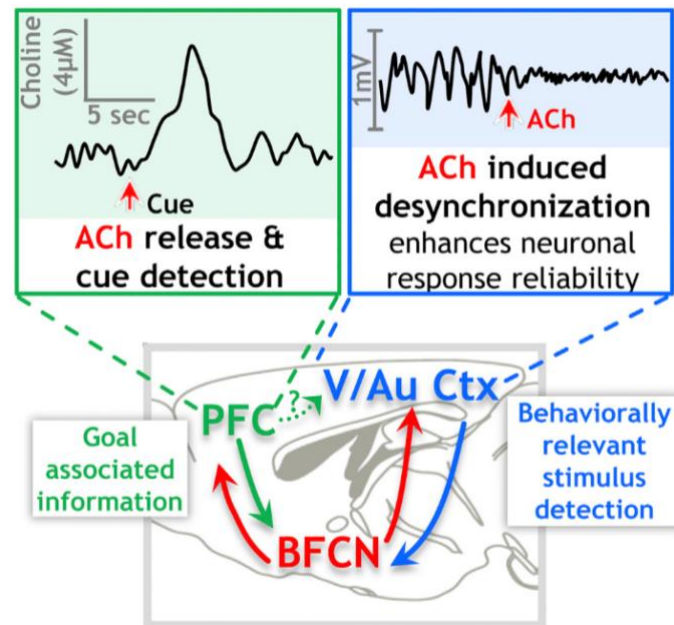
Figure 8: Cholinergic Neuromodulation of Cortical Attention Circuitry

The PFC is essential for task-relevant attentional shifts (also referred to as "top-down" regulation). Circuitries between the PFC, BFCN and sensory cortex eventually lead to enhanced cortical neuronal response reliability and cue detection through prefrontal, phasic ACh release [24,47]

Abbreviations: PFC – prefrontal cortex; V/Au Ctx – visual / auditive cortex; BFCN – basal forebrain cholinergic neurons

Bloem et al. precisely describe this process as a "combination of reduced lateral interactions and increased sensitivity to thalamic inputs [enhancing] the networks sensitivity to incoming information".[48] Cholinergic signaling is therefore vital for the incorporation of newly detected stimuli in an individual's behavior by promoting an enhanced arousal state as well as for the detection of salient cues themselves.

4.5.2 Cholinergic Neuromodulation and Reward

Obesity and addiction share similar features such as alterations in mesolimbic reward signaling in regards of the consumption of palatable food items or substances of abuse, respectively.[23] Here, cholinergic neuromodulation of dopaminergic projections plays a crucial role. The main neuronal mesolimbic pathways originate from the ventral tegmental area (VTA), which is situated in midbrain, to basal forebrain structures, most importantly the striatal nucleus accumbens (NAc).[23] Fast increases of dopamine release, triggered by drugs of abuse or other rewarding stimuli such as palatable food, are associated with the pleasant feeling, also referred to as "high".[22]
Cholinergic projections from the pedunculopontine-lateral dorsal tegmental nuclei from the brainstem innervate dopaminergic neurons in the VTA and predominantly change neuronal (dopaminergic) excitability, and coordinate the firing of these neurons (Figure 9).[38]
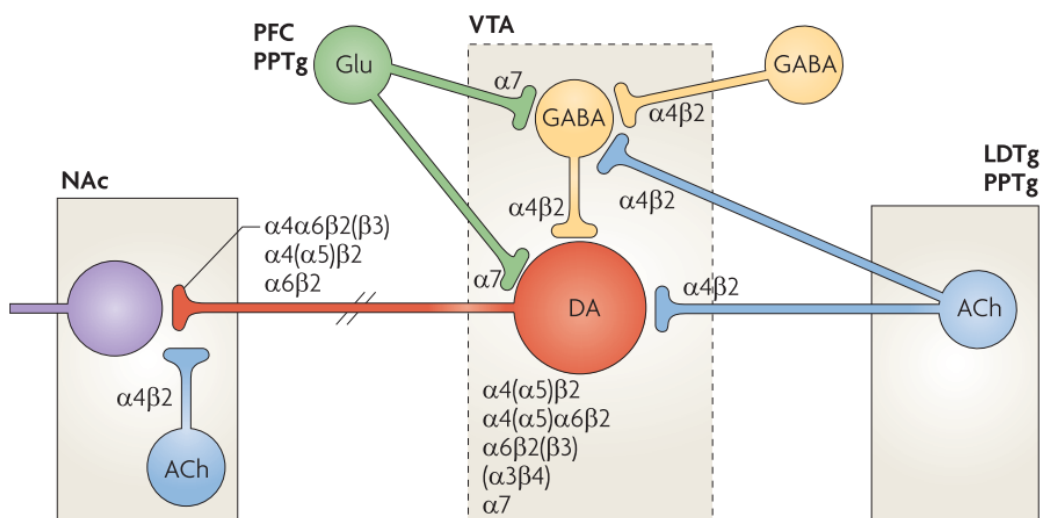
Figure 9: Cholinergic Neuromodulation of the Mesolimbic Reward Pathway

Different nAChRs shape dopaminergic, mesolimbic signaling through interaction with other GABAergic and glutamatergic neurons

Abbreviations: NAc – nucleus accumbens; PFC –prefrontal cortex; PPTg - pedunculopontine-lateral dorsal tegmental nuclei; VTA – ventral tegmental area; LDTg – lateral dorsal tegmental group of neurons

Mesolimbic dopaminergic neurons at resting state show a tonic (1-8Hz), low frequency firing pattern, whereas external stimuli lead to phasic (>15Hz) neuronal firing, which is essential for reward and goal motivated behavior signaling.[23]

Both sucrose as well as nicotine increase dopaminergic firing activity in the mesolimbic reward system.[49] Here, the α4β2 nAChR subunit seems to be notably essential for DA release.[23] Avena et al. showed that antagonizing the nAChR with mecamylamine substantially reduced dopamine release in the mesolimbic system after administration of cocaine.[50] Interestingly, in rats long-term diets high in sucrose lead to an increase of extracellular ACh, accumbal α4β2 nAChR density as well as a decrease of dopamine in the NAc shell, pointing out to neurotransmitter imbalances as potential reasons for suffering from withdrawal symptoms or higher incentive salience value of food items or substances of abuse, respectively.[51,52]

Individuals with obesity or substance abuse disorder both show a downregulation of dopamine D2 receptors (D2R) in the striatum and these D2R on cholinergic interneurons modulate the tonic-phasic firing patterns in response to salient cues, interacting with nAChR on presynaptic dopaminergic neurons.[53]

Moreover, in rodents, higher levels of impulsivity are associated with D2R downregulation.[22] Blendy et al.[8] showed that smokers with obesity have lower rewarding effects from smoking cigarettes than non-obese participants.

In rats, intracranial self-stimulation (ICSS) with nicotine administration remarkably changed their sensitivity of their brain reward system, persisting for at least 36 days after administration.[54] Kenny and Markou et al.[54] proved that this aforementioned change could be antagonized by high-affinity nAChR antagonist dihydro-β-erythroidine (DHβE; 3 mg/kg), highlighting the receptor's relevance in this process. This so called "reward hypersensitivity" could substantially add to enhanced weight gain after smoking cessation using palatable food items as reward replacements instead of consuming nicotine.[54] In total, smoking, endogenous cholinergic signaling as well as distinct eating habits have great, longer lasting impact on mesolimbic reward signaling.

4.5.3 Cholinergic Neuromodulation and Eating Behavior

Administration of nicotine as well as endogenous cholinergic signaling vastly influence central structures regulating appetite as well as body homeostasis. The hypothalamus plays a key role in body homeostasis regulation containing several neuronal areas, amongst others the ventromedial hypothalamus nuclei (VMH), responsible for appetite suppression, and the lateral hypothalamus nuclei (LHA), responsible for the stimulation of appetite.[30] Interestingly, within the VMH lie another group of nuclei, called the arcuate nuclei (ARC) which in turn contain central neurons mediating homeostasis: on the one hand, the anorexigenic, i.e. appetite-depressing, proopiomelanocortin (POMC) neurons and cocaine- and amphetamine-regulated transcript (CART) neurons. On the other hand, the ARC also contain the orexigenic, i.e. appetite-stimulating, neuropeptide Y (NPY) and agouti-related peptide (AgRP) neurons (Figure 10).[30]
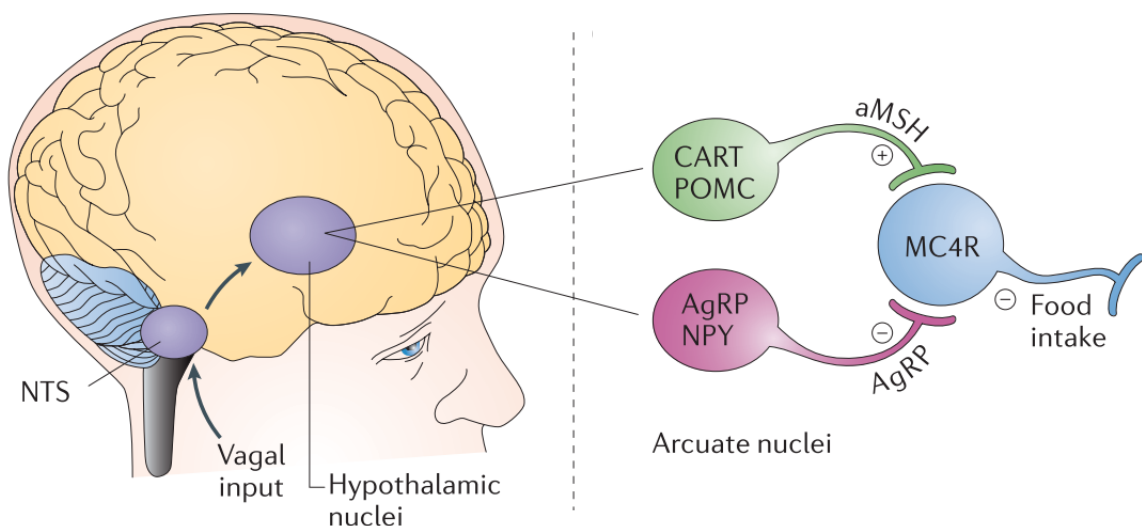
Figure 10: Homeostatic Appetite Regulation Signaling

Both orexigenic and anorexigenic group of neurons project to the melanocortin 3 and 4 (MC3R, MC4R) receptor. CART and POMC neurons do so by POMC cleavage product α-melanocyte-stimulating hormone (αMSH) and thereby activating MC4R, which leads to decreased food intake. On the contrary, orexigenic neurons inhibit MC4R, which in turn leads to increased food intake.[55] The nucleus tractus solitarii (NTS), devoid of a blood-brain-barrier (BBB), mediates peripheral homeostatic signals[49]

Through activation of POMC neurons, nicotine decreases food intake and increases energy expenditure through stimulation of central β4 nAChR.[56] Also, enhanced ACh levels in the NAc increase satiety. In rats, accumbal administration of neostigmine, which inhibits the AChE and therefore functions as a cholinergic agonist, dose-dependently decreases food intake compared to control rats.[50] Ablation of basal forebrain diagonal band of Broca (DBB) cholinergic neurons in mice through Cre-dependent14 adeno-associated virus (AAV), leads among other effects to higher average body fat, lean mass, and higher average insulin, leptin and blood cholesterol levels.[57]

Moreover, in a fMRI study Kroemer et al.[58] showed that nicotine decreases functional coupling of homeostasis-regulating neurons in the hypothalamus and reward-mediating neurons in the basal forebrain during the reaction to palatable food cues, apparently reducing their incentive salience potential.

4.6. Positron Emission Tomography (PET) as a Molecular Imaging Technique for Measuring nAChR *In Vivo*

4.6.1 PET Imaging

PET is a molecular imaging technique applying radiotracers that are radioactive-labeled molecules for measuring receptor and cell function.[59]

Tissue distribution of the tracer depends on variables such as cerebral blood flow, plasma clearance, as well as receptor affinity and quantity, therefore kinetic models are applied to analyze specific time-activity data.[60] Here, the outcome measure (or the receptor availability) is usually the binding potential (BP) representing an index of the relative number of unoccupied receptor sites.[61] Interpretations of PET studies should consider that the BP can rise in case of an increase of receptors as well as a decrease of endogenous receptor ligands. To account for differences in tracer distribution, often the *Volume of distribution* (V_T) is applied: C_T / C_P (tissue ($kBq \cdot cm^{-3}$) / fraction of radiotracer in plasma at (pseudo-)equilibrium ($kBq \cdot mL\text{-}1$)).[62]

Since PET data offers limited spatial resolution, additional or simultaneous magnetic resonance imaging (MRI) provides robust anatomical co-registration. Furthermore, the combination of PET and functional MRI (fMRI), allows *in vivo* imaging of the dynamics of central receptor signal transmission.[17]

4.6.2 Imaging of α4β2 Nicotinic Acetylcholine Receptors

Receptor density of α4β2 nAChR in human CNS is moderately low, making the production of a radiotracer with sufficient brain kinetics and acceptable binding potential quite demanding.[63] For many years [^{11}C]nicotine as the first radiotracer[64], and then 2-[^{18}F]FA ((S)-3-(azetidin-2-ylmethoxy)-2-[^{18}F]fluoropyridine) and 6-[^{18}F]FA ((S)-3-(azetidin-2-ylmethoxy)-6-[^{18}F]fluoropyridine) have been the commonly used radiotracers for imaging the nAChR (Figure 11).[65] Disadvantages with these tracers are e.g. high nonspecific binding while specific binding is low, and rapid metabolism for [^{11}C]nicotine. While showing good specific binding, further limitation included slow brain uptake and washout rates for 2-[^{18}F]FA and 6-[^{18}F]FA.[65] Hence, acquisition times of up to 6-7 hours are mandatory. Clinical applications are therefore in need of improvement. Nonetheless, due to the lack of better alternatives, imaging studies with 2-[^{18}F]FA to examine the nAChR have still been conducted until recently.[66,67]
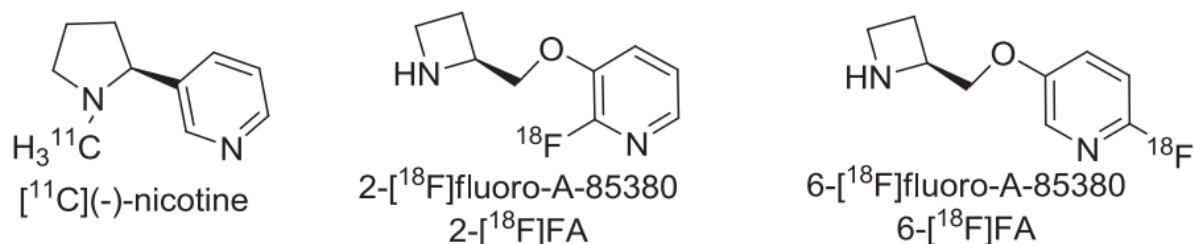
Figure 11: Established Radiotracers for α4β2 nAChR PET Imaging

With the development of [18F]nifene and [18F]AZAN (Figure 12) two new radiotracers proved superiority compared to 2-[18F]FA in terms of tracer kinetics and shorter time frames in scanning procedures in quantitative α4β2 nAChR imaging.[65] [18F]nifene is an α4β2 nAChR agonist with specific regional binding and fast kinetics, reaching transient equilibrium at approximately 30-45 minutes, and therefore 7-fold shorter compared to 2-[18F]FA. Preclinical baboon studies highlighted the suitability of [18F]nifene for human studies, even though one must mention the relatively high demands in radiosynthesis.[65]
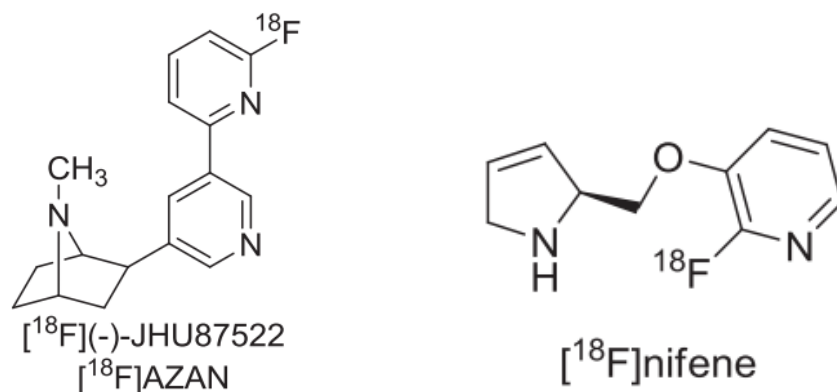
Figure 12: [18F]AZAN and [18F]Nifene

[18F]AZAN, which is an α4β2 nAChR antagonist, also demonstrates high non-displaceable binding potential (BP_{ND}) and V_T values as well as rapid brain kinetics, reaching steady-state within 90 minutes after injection time.[32] Due to its lipophilic character [18F]AZAN efficiently penetrates the blood-brain barrier. Blocking studies with cystisine, an α4β2 nAChR selective agonist, varenicline, a partial a α4β2 nAChR

agonist, as well as nicotine highlighted substantially lower brain uptake in baboon[32] and human[63] brain due to competitive receptor binding. This also shows [18F]AZAN's sensitivity to a potential change in the endogenous ACh pool.

4.6.3 (-)-[18F]flubatine: a specific α4β2 nAChR radiotracer

In this study, a new, second-generation radioligand for α4β2 nAChR imaging was applied. (-)-[18F]flubatine which was earlier known as (-)-[18F]NCFHEB ((−)-[18F]norchloro-fluoro-homoepibatidine)[68], is a less noxious derivative of epibatidine. It was developed and clinically validated in Leipzig.[68,69] There are two known enantiomers (+)-[18F]flubatine and (-)-[18F]flubatine (Figure 13).[70,71]

[a](+)-[18F]flubatine   [b](-)-[18F]flubatine
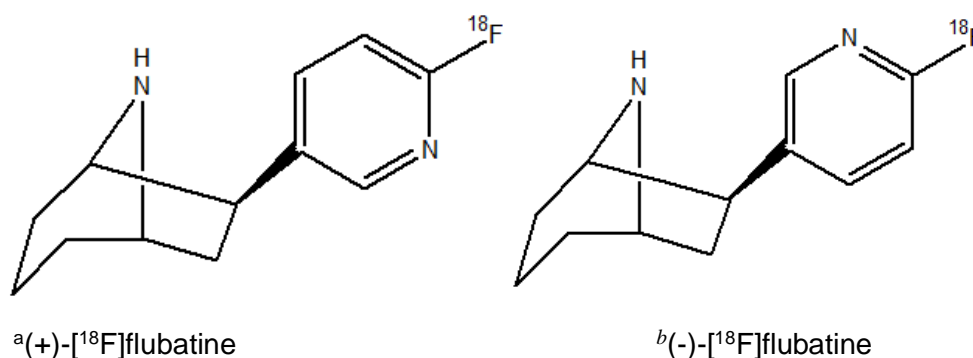
Figure 13: Both (+)-[18F]flubatine and (-)-[18F]flubatine Enantiomers

[a]Adapted by permission from: Springer Science+Business Media, European Journal of Nuclear Medicine and Molecular Imaging, (+)-[18F]Flubatine as a novel α4β2 nicotinic acetylcholine receptor PET ligand-results of the first-in-human brain imaging application in patients with β-amyloid PET-confirmed Alzheimer's disease and healthy controls, Tiepolt et al. 2020, licensed under a Creative Commons Attribution 4.0 International License, http://creativecommons.org/licenses/by/4.0/

[b]Adapted by permission from: John Wiley & Sons, Journal of Labelled Compounds and Radiopharmaceuticals, (-)-[18F]Flubatine: evaluation in rhesus monkeys and a report of the first fully automated radiosynthesis validated for clinical use, Hockley et al., © 2013

The improved tracer properties of newly developed (-)-[18F]flubatine with faster brain kinetics, high binding properties and preferable parent compound metabolism have been shown in several consecutive studies:

Firstly, Gallezot et al.[72] preclinically proved a dose-dependent reduction in (-)-[18F]flubatine binding (V_T/f_P) in rhesus monkeys with two acetylcholinesterases (AChE), which leads to an increase of ACh, inhibiting its hydrolysis. This indicates the sensitivity of the radiotracer for measuring endogenous ACh changes (Figure 14).
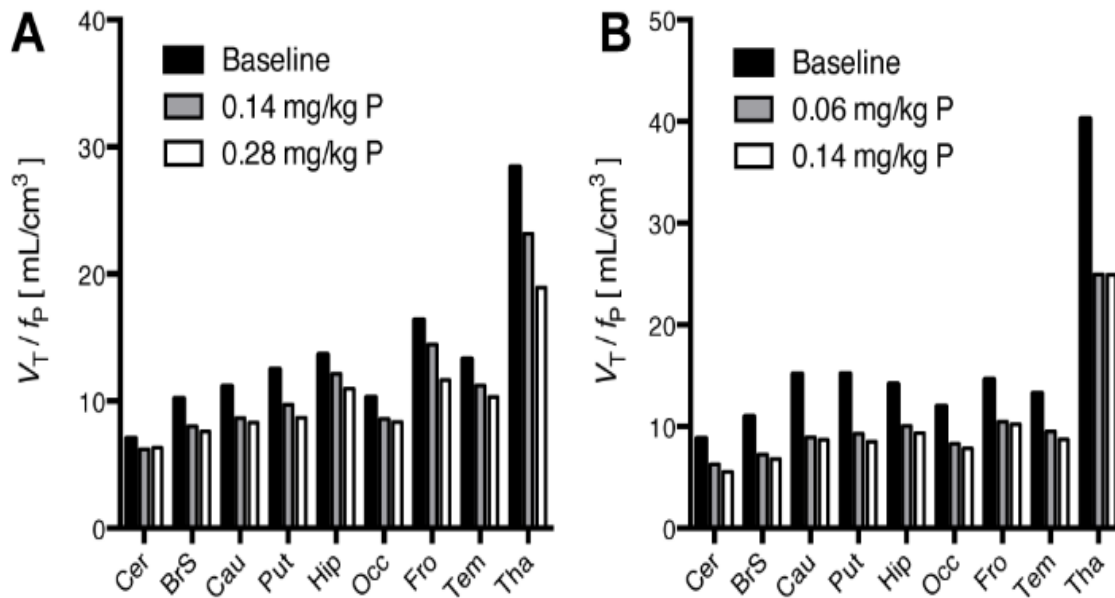
Figure 14: (-)-[^{18}F]flubatine's Sensitivity to Endogenous ACh Changes

Dose-dependent reduction of radiotracer binding, induced by AChE in animal A and B (rhesus monkeys)

Adapted by permission from: John Wiley & Sons, Synapse, Evaluation of the sensitivity of the novel α4β2* nicotinic acetylcholine receptor PET radioligand ^{18}F-(−)-NCFHEB to increases in synaptic acetylcholine levels in rhesus monkeys, Gallezot et al., © 2014

Both AChE physostigmine and donepezil induced binding reduction effects in the aforementioned non-human primates: for physostigmine bolus plus infusion injection (0.06-0.28 mg/kg) with decreased binding of 18%–38% in thalamus, 22–43% in basal ganglia, and 15–33% in cortex; and for donepezil bolus injection (0.25 mg/kg), binding was reduced by 14% in the thalamus, 17–20% in the basal ganglia, 9–14% in the cortex, respectively.[72] The heterogeneity in reduction most likely stems from known interactions of anesthetic agents (ketamine, isoflurane) with ACh release[72] and was also reported in other studies.[73,74]

Then, Sabri et al.[68] conducted the first-in-human application to proof the use of (-)-[18F]flubatine as an alternative for tracers with slow kinetics, such as 2-[18F]FA. This trial represents the successful translation from animal studies to application in humans. (-)-[18F]flubatine exhibits rapid kinetics, especially in cortical areas, as cortical tracer delivery rates are eminent and V_T can be estimated here within 30 minutes using a simple 1-tissue-compartment model (1TCM).[68] For all regions of interest (ROI), (for exemplary analysis, see 6. Materials and Methods), estimation of V_T can be achieved within a 90-minutes time frame. The radiotracer shows a very stable metabolism with high percentage of parent compound in blood plasma, as can be apprehended in Figure 15.
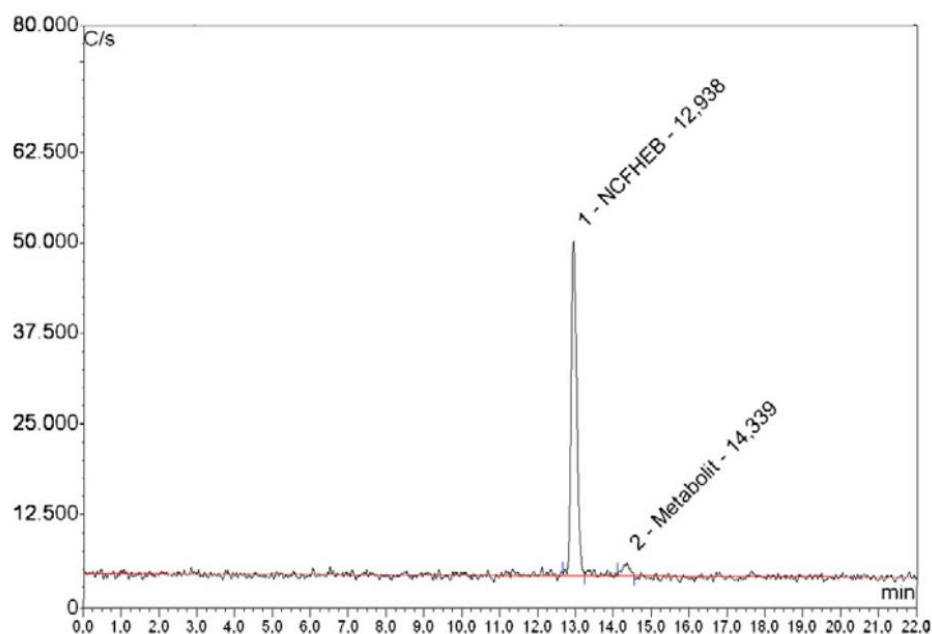
Figure 15: Metabolism of (-)-[18F]flubatine

Chromatographic analysis (radio-HPLC) highlights slow degradation and high proportion of parent compound in blood plasma

The fast kinetics of (-)-[18F]flubatine are demonstrated in the plasma time-activity curves (TACs) (Figures 16 and 17) of the thalamus, frontal cortex and the reference region corpus callosum describing an early initial peak and slow tracer concentration decrease until 270 min.[69] In TACs the time (x-axis) is plotted against the measured tissue or plasma activity (y-axis).
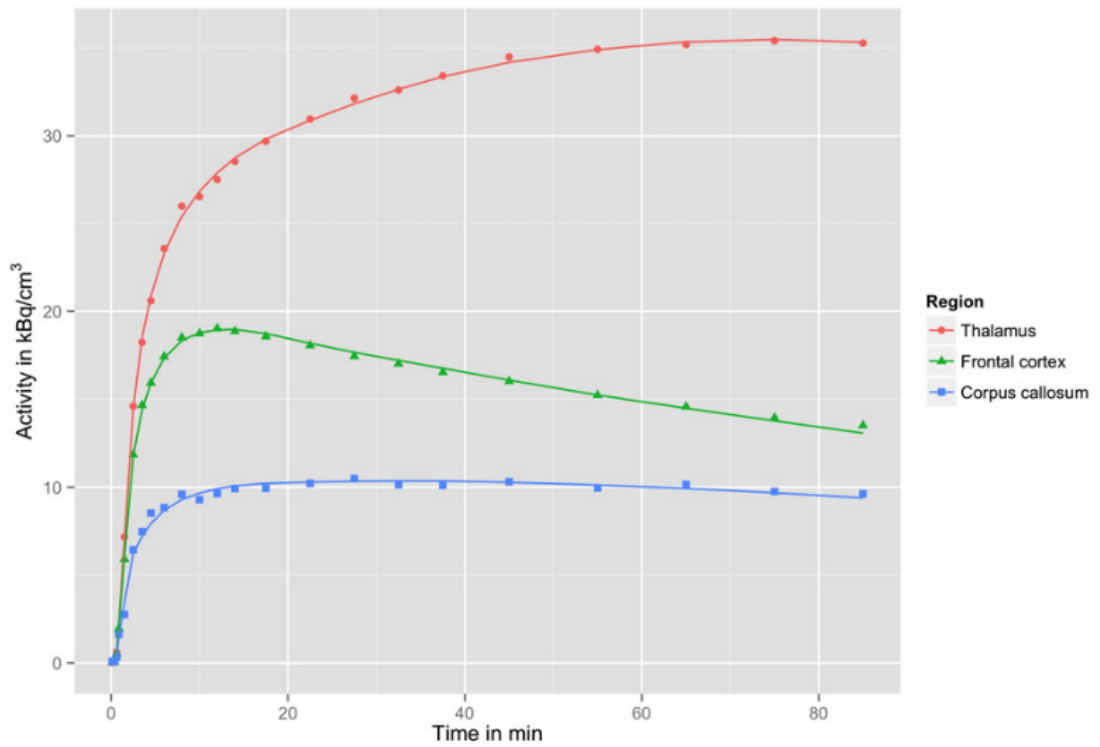
Figure 16: TACs of (-)-[^{18}F]flubatine (Blood Plasma, 0-90min)
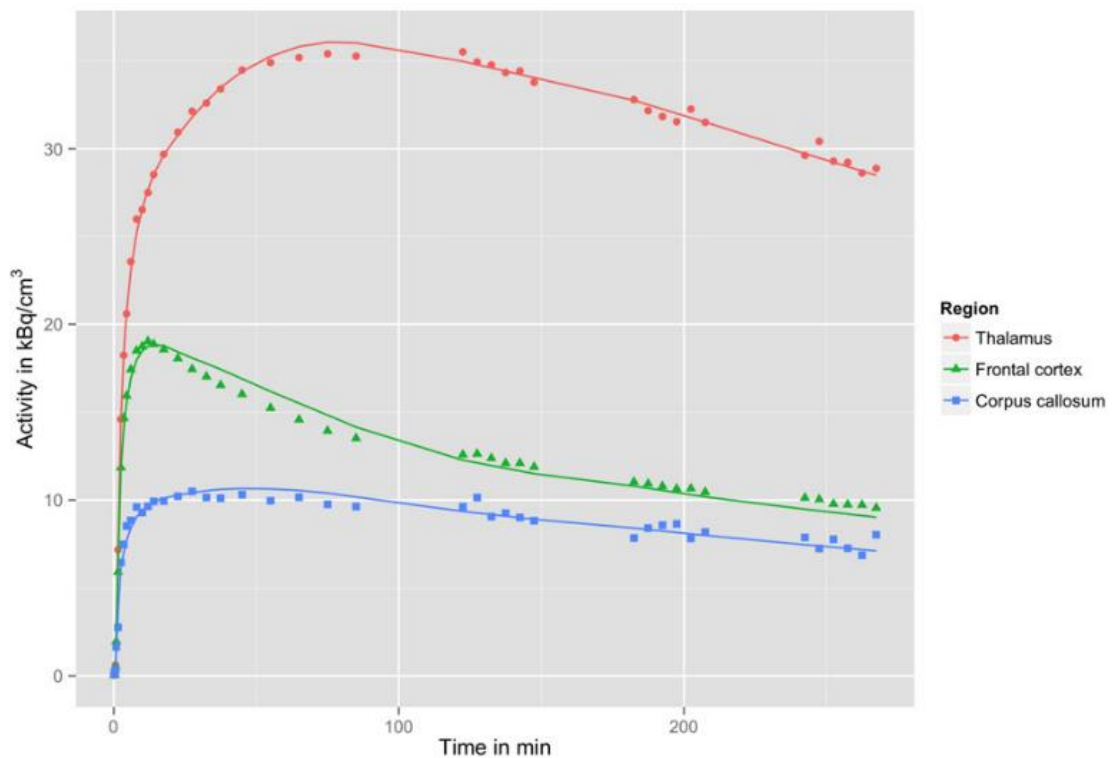
Figure 17: TACs of (-)-[^{18}F]flubatine (Blood Plasma, 0-270min)

Figure 16+17: Reprinted from: NeuroImage, 118, Sabri et al., First-in-human PET quantification study of cerebral α4β2* nicotinic acetylcholine receptors using the novel specific radioligand (−)-[^{18}F]Flubatine, 199-208, © 2015, with permission from Elsevier

Following the normal distribution of α4β2 nAChR density (Figure 18) in the brain, V_T in the thalamus (27.44±3.77) exhibits highest values, followed by midbrain, striatum and cerebellum (e.g., putamen: 12.70 ± 0.87), then cortical regions (e.g., frontal cortex: 10.02 ± 0.83), and lowest in the corpus callosum (6.31 ± 0.80).[68]
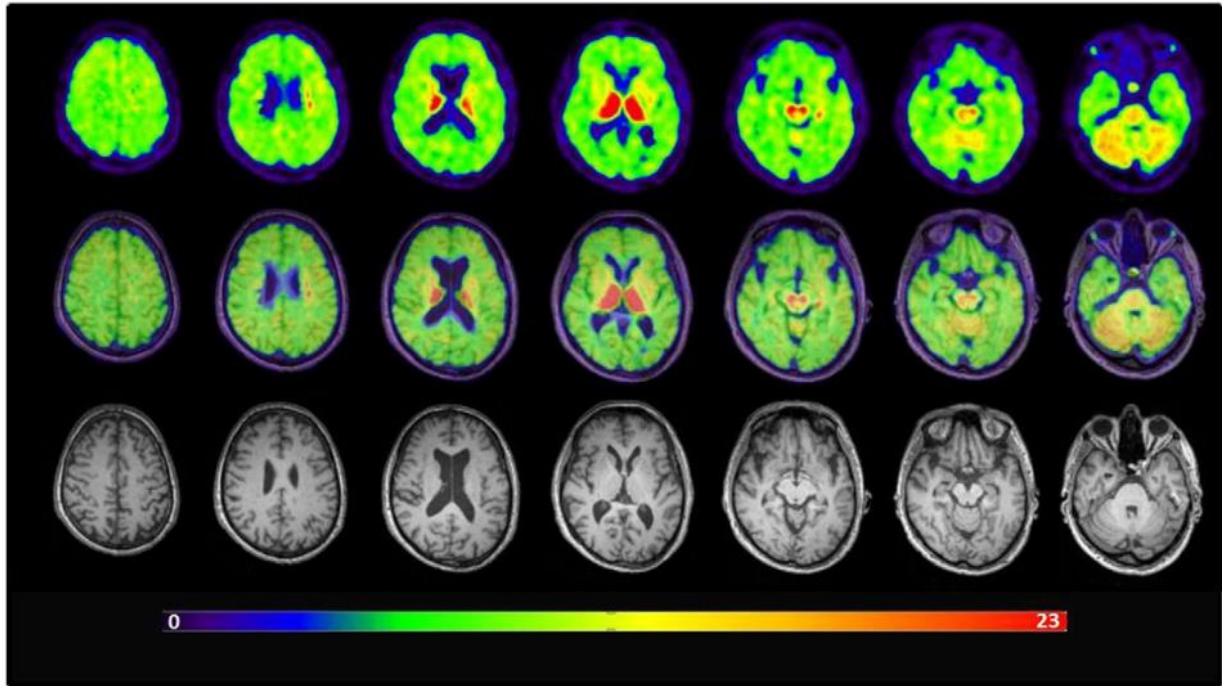
Figure 18: α4β2 nAChR Distribution in the Human Brain

Parametric, transaxial (-)-[18F]flubatine imaging in one healthy subject

upper row: PET images of distribution volume (V_T); middle row: co-registered PET/MRI; lower row: T1-MRI images

Another important milestone in the development of imaging approaches with (-)-[18F]flubatine was the work of Hillmer and colleagues from Yale University, New Haven, CT. Hillmer et al. tested a bolus plus constant infusion protocol with (-)-[18F]flubatine administration as well as its sensitivity to endogenous ACh changes in humans with a physostigmine challenge.[75]

Figure 19 describes the bolus plus constant infusion paradigm, illustrating an establishment of true equilibrium after approximately 120 min between radiotracer in tissue at receptor site and in plasma. One big advantage of studying receptor binding at true equilibrium in a single-scan (bolus-infusion) approach is the potential to observe slight changes in binding to eventually relate this to changes in neurophysiological processes, like enhanced endogenous neurotransmitter release. Changes in the TACs can then be referred to given stimuli (e.g. visual food cues). Taking regions under account that apparently do not reach true equilibrium after 120 minutes post injection, Hillmer et al. also suggested a *tissue clearance correction* (TCC*).*[76]
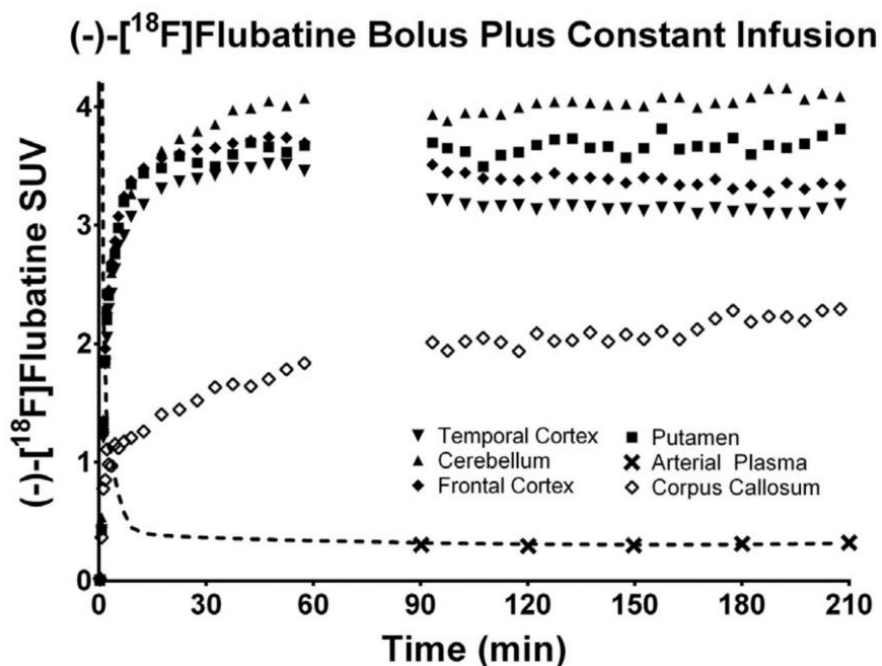
Figure 19: Bolus Plus Infusion Protocol

Time (x-axis) is plotted against (-)-[18F]flubatine (y-axis) standard uptake value (SUV).

Abbreviations: SUV: describes the ratio of regional radiotracer compared to whole-body radioactivity concentration and is therefore a relative quantification measurement of specific radiotracer uptake.[77]

Reprinted from NeuroImage, Vol. 141, Hillmer et al., Imaging of cerebral α4β2* nicotinic acetylcholine receptors with (-)-[18F]Flubatine PET: Implementation of bolus plus constant infusion and sensitivity to acetylcholine in human brain., 71-80, © 2016, with permission from Elsevier

In the following, Hillmer et al. showed a stable metabolism in humans with high proportions of parent compound in plasma (Figure 20).
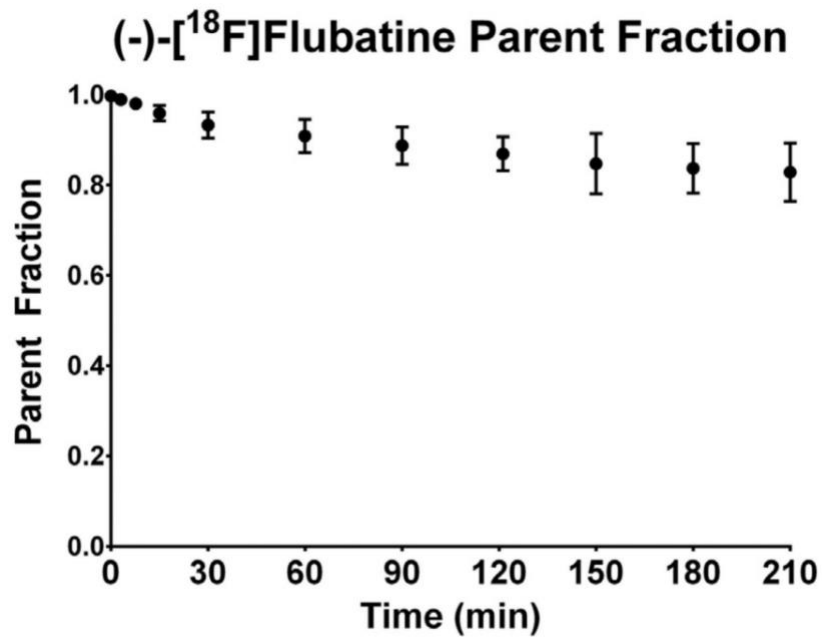
Figure 20: Parent Fraction of (-)-[^{18}F]flubatine

After 90 min still almost 90% and after 210 min almost 80% remains of unchanged parent compound.

To evaluate (−)-[^{18}F]flubatine's sensitivity to changes in endogenous ACh levels, a physostigmine challenge in humans was conducted in a two-scan (bolus injection), as well as in a single-scan bolus-infusion paradigm, lead to small, but significant changes in V_T / f_P [75], as depicted in Figure 21.
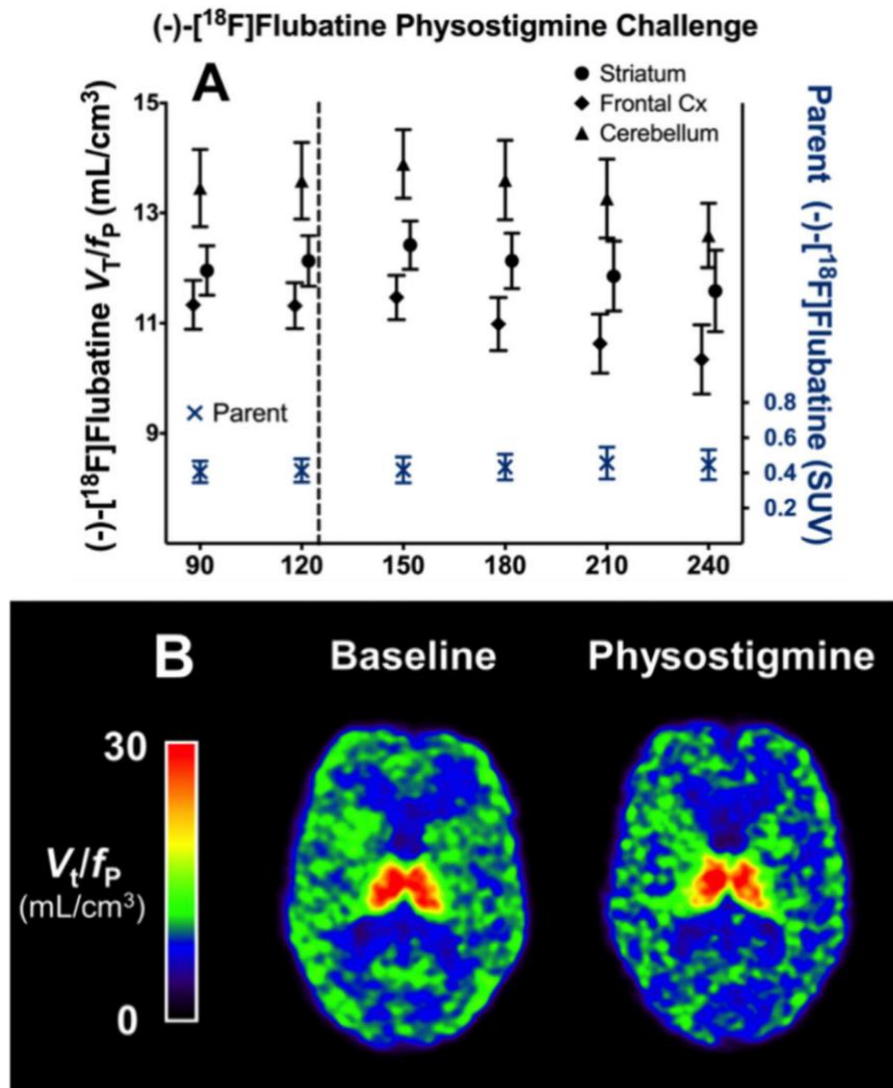
Figure 21: (-)-[18F]flubatine Physostigmine Challenge

Part A: Changes in (-)-[18F]flubatine: Physostigmine challenge (1.5mg) after 125 min lead to a decline in V_T/f_P in depicted brain areas (Striatum, Frontal Cx, Cerebellum), with stable parent compound metabolism in arterial plasma (blue dots)

Part B: Changes in (-)-[18F]flubatine binding from baseline (110-130 min) to post-challenge (200-220 min); voxel-wise (-)-[18F]flubatine V_T/f_P images[75]

Abbreviations: Frontal Cx: Frontal Cortex; SUV: Standard Uptake Value

To conclude, the work by Hillmer et al. provided evidence that the bolus-infusion administration protocol is suitable for quantification of V_T at fast kinetic rates (equilibrium at 120 min) and further highlights (-)-[18F]flubatine's sensitivity to changes in endogenous ACh levels.

4.7 Volumes of Interest (VOI)

According to recent literature we examined pivotal brain regions with cholinergic neuromodulation (Table 2) which are involved in reward and attentional signaling.

Table 2: Preselected Brain Regions with Neurophysiological Function

Volumes of Interest (VOI)	Neurophysiological function
Amygdala	Modulation of emotional and affective state as well as memory and attention[78]
Head of Caudate (Nc. Caud.)	Important region in goal-directed action selection circuitry as well as motor function[79]
Hypothalamus (HPT)	Regulation of body homeostasis e.g. in terms of feeding, which is critically modulated by cholinergic signaling[49]
Insula	Multifunctional structure including processing of salient cues, regulation of affective states as well as interoceptive awareness[80]
Nucleus Accumbens (NAc)	Plays a pivotal role in mesolimbic reward signaling, e.g. computing food reward stimuli whilst undergoing cholinergic neuromodulation[50,51]
Nucleus Basalis of Meynert (NBM)	Part of the basal forebrain, responsible for the majority of cholinergic innervation of almost the entire corticle mantle[38]
Orbitofrontal Cortex (OFC)	Assessment of reward value of sensory input as well as flexible behavioral adaptation in regards to stimulus-response paradigms[81]
Prefrontal Cortex (PFC)	Executive control center responding to external and internal input with apt behavioral responses[82]
Thalamus	Encloses vast amount of nAChR[68]; crucial role in processing of sensory information as well as action-selection circuitry involving cholinergic neuromodulation responding to external cues[83]
Ventral Tegmental Area (VTA)	Plays a central role next to NAc in mesolimbic reward signaling, which is greatly modulated by cholinergic neurons[50]

5. Objective

Cholinergic modulation of basal forebrain, thalamocortical as well as mesolimbic networks has a pivotal role in cognitive function such as attention and information processing about salience and reward signaling. This implies that changes in ACh transmission may lead to altered cognitive control that augments altered eating behavior leading to obesity. The aim of the present study was therefore to investigate biological mechanisms of cholinergic neurotransmission, specifically the α4β2 nAChR as a potential pharmacological target in obesity.

The α4β2 nAChRs availability was quantified by means of PET and the highly α4β2 nAChR-selective radioligand (-)-[^{18}F]flubatine under baseline and stimulus conditions (salient visual food stimuli) in order to assess changes of central cholinergic activity in individuals with obesity (OB) and normal weight (NW). Thereby, regional availability of α4β2 nAChR was measured by applying VOI-based analyses to calculate V_T of (-)-[^{18}F]flubatine from PET data as the primary outcome measure.

1.) **The primary hypothesis** of the study is that **α4β2 nAChR availability is higher in OB participants compared with NW controls** under baseline and stimulus conditions in brain regions important for:
   - cue detection, the generation of attention and motivational brain responses such as NBM, PFC, OFC, the head of the caudate and the thalamus
   - mesolimbic reward signaling such as the VTA and NAc
   - neuromodulation of affective states, interoceptive awareness as well as energy homeostasis such as the amygdala, insula and the HPT
2.) **The secondary hypothesis** is that changes in eating behavior scores on a **visual analogue scale (VAS)** are **correlated** with changes in **α4β2 nAChR availability. The relationship differs** between **resting state and stimulus conditions** in both NW as well as OB.

These data together should provide hints towards an association between the α4β2 nAChR availability and cognitive function such as attention, the processing of salience information and hedonic eating as neurobiological underpinnings of obesity. This will help to frame future intervention strategies in individuals with the propensity to develop obesity.

6. Materials and Methods

6.1 Ethics statement

This study was approved by the *Bundesamt für Strahlenschutz (BfS)* / Federal Office for Radiation Protection, local ethics committee of the Medical Faculty of the University of Leipzig (225/15-ek) and complies with the 1964 Declaration of Helsinki including current revisions. It follows the guideline for Good Clinical Practice (GCP) and is registered at the *Deutsches Register für klinische Studien* (DRKS) under DRKS00010927.

6.2 Study Design

The (-)-[^{18}F]flubatine PET/MR imaging study was a prospective, open, proof-of-concept, monocentric phase 0/I study. Study participants completed three visits (Figure 22) including screening examination (Visit 0) and telephone follow-up (Visit 3).
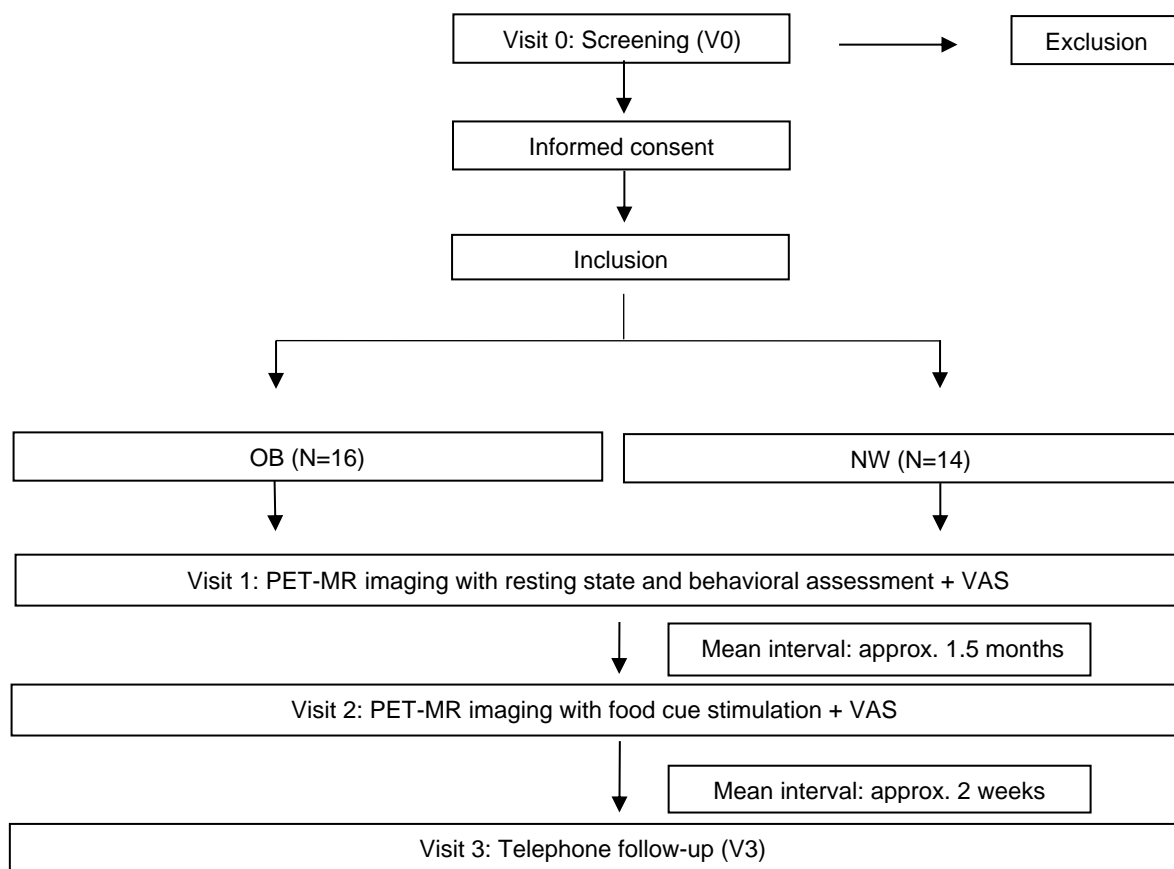
Figure 22: Study Design Flowchart

Abbreviations: OB: participants with obesity; NW: normal-weight participants; VAS: visual analogue scale assessing current state of emotions such as craving, hunger or sadness after each examination/visit

At screening visit (V0) information regarding personal data case history and concomitant diseases were received. Before each examination day (baseline and stimulus), brief clinical history and physical examination was conducted. To exclude eating disorders or manifest depression, we applied Beck Depression Inventory (BDI) and Eating Disorder Examination Questionnaire (EDE-Q8). Pregnancy was further excluded by β-hCG testing.

6.3 Study participants

Recruitment of participants included public postings and ecotrophological consulting meetings at the University Medical Center Leipzig (UKL). The whole study population consisted of 30 participants. Data acquisition was carried out in 14 NW (N=14; mean BMI 21.8±1.90 kg/m^2; 11 females; mean age 28.1±7.58 years; ranging from 19-45 years) and 16 study participants with OB (N=16; mean BMI 37.8±3.18 kg/m^2; 10 females; mean age 40.6±14.0 years; ranging from 20-62 years). All recruited individuals were non-smokers. Exclusion and inclusion criteria were applied to assess eligibility of study participants and a drug screening was conducted to ensure that no illicit substances that interfere with brain states and applied radiotracer were taken. Informed consent was obtained in each study participant. NW with TFEQ disinhibition score ≥8 were ruled out from study participation.[84,85] Other inclusion and exclusion criteria comprised:

Inclusion Criteria

- OB BMI ≥30 kg/m^2
- NW BMI ≤25kg/m^2
- Age: 18-65 years
- Sex: male and female
- Non-smoker
- Written informed consent
- Body shape to fit in MRI scanner

Exclusion Criteria

- Neurological / neuropsychiatric disorders stated in case history
- Neurosurgical operations in the past
- Structural brain lesions (stroke, trauma, etc.)
- Permanent use of psychotropic drugs
- Alcohol and substance abuse (checked through conducted drug screenings)
- Severe psychotic disorders and/or communicational deficits, that could affect informed consent
- Simultaneous participation in other clinical investigations
- General contraindications for nuclear medical examination, such as pregnancy or breastfeeding women, or for MRI (claustrophobia, heart pacemakers, ferromagnetic applications, etc.)
- Vegan nutrition habits

6.4 Visual Analogue Scale (VAS)

To obtain data on satiety state and hunger, feeling of disinhibition of eating, i.e. loss of control, or feelings of craving during the scans, the VAS was filled out after baseline and stimulus examination. The continuum at hand (Figure 23) was translated into numbers ranging from 0 ("not at all") to 100 ("extremely") and correlated with calculated V_T of (-)-[^{18}F]flubatine.

Not at all	immensely
0	100

1) Are you currently
   hungry?

2) Are you currently
   craving for food?

3) Are you currently
   experiencing a loss of control
   of your eating habits?

4) Are you full, i.e. experiencing
   current state of satiety?

5) Do you think
   food is tasty?

Figure 23: Visual Analogue Scale

Self-assessment of current satiety state, cravings for food or loss of control

6.5 PET/MR Imaging

The α4β2 nAChR radioligand (-)-[^{18}F]flubatine was applied twice on separate days, i.e. under baseline (resting state) and stimulus conditions, using the bolus-infusion protocol previously established by Hillmer et al.[75] (4.6.3 (-)-[^{18}F]flubatine: a specific α4β2 nAChR radiotracer). Each scan was carried out with a truly simultaneous PET/MR imaging scanner (*Biograph mMR*; Siemens Healthineers, Erlangen*).* Radiotracer was synthesized using the synthesis module *TRACERlab FX FN* (General Electric Healthcare) under GMP conditions according to Patt el al..[86] Two intravenous cannulae were administered before each scan, one for the application of radiotracer, the other for intravenous blood sampling. The total scanning duration was 165 minutes, subdivided in two data acquisition time frames: from 0 to 60 minutes p.i. and, after having reached radiotracer equilibrium, from 120 to 165 minutes post injection. Before radiotracer application, MR imaging UTE (ultra-short echotime) sequence for attenuation correction was conducted.

In total, approximately 300 MBq of (-)-[^{18}F]flubatine was applied per scan. Each scan started with a 90-second bolus administration (10 ml; administered activity in NW, mean: 195±26 MBq; in OB, mean: 202±4 MBq), followed by constant tracer infusion (98 ml, infusion rate of 0.6 ml/min; NW, mean: 89±14 MBq; OB, mean: 91±1 MBq). During the first time frame of each visit, we carried out three-dimensional list mode acquisition for PET data and T1-weighted MP-RAGE (echo time: 2.53 ms, repetition time: 1900ms, inversion time: 900 ms) to obtain anatomical data for imaging data co-registration and to rule out neuroanatomical abnormalities. The acquired PET data were reconstructed into a 256 × 256 matrix (voxel size: 1.0 × 1.0 × 2.03 mm^3) using the built-in 3D ordered subset expectation maximization algorithm with 8 iterations, 21 subsets and a 3-mm Gaussian filter. Standard corrections for decay, scatter, dead time, and attenuation were performed.[87] Figure 24-26 depict radiotracer application according to the bolus-infusion protocol, starting with (-)-[^{18}F]flubatine bolus. After 60 minutes, study participants left the scanner while still receiving radiotracer infusion to reach radiotracer equilibrium after 120 minutes post injection.

<u>Visit 1: Baseline Assessment (V1)</u>

At 120 minutes p.i. fMR imaging data (EPI, echo-planar imaging) and structural MR imaging data (T1 MP-RAGE) together with three-dimensional list mode PET data acquisition was carried out (Figure 24). Scan ended at 165 minutes post injection.

Time (minutes)	Before V1	0-60	60-120	120-165
Scanner	IN	IN	OUT	IN
MR Imaging	UTE	T1-MP-RAGE	-	UTE,EPI,T1-MP-RAGE
PET	-	List-mode	-	List-mode
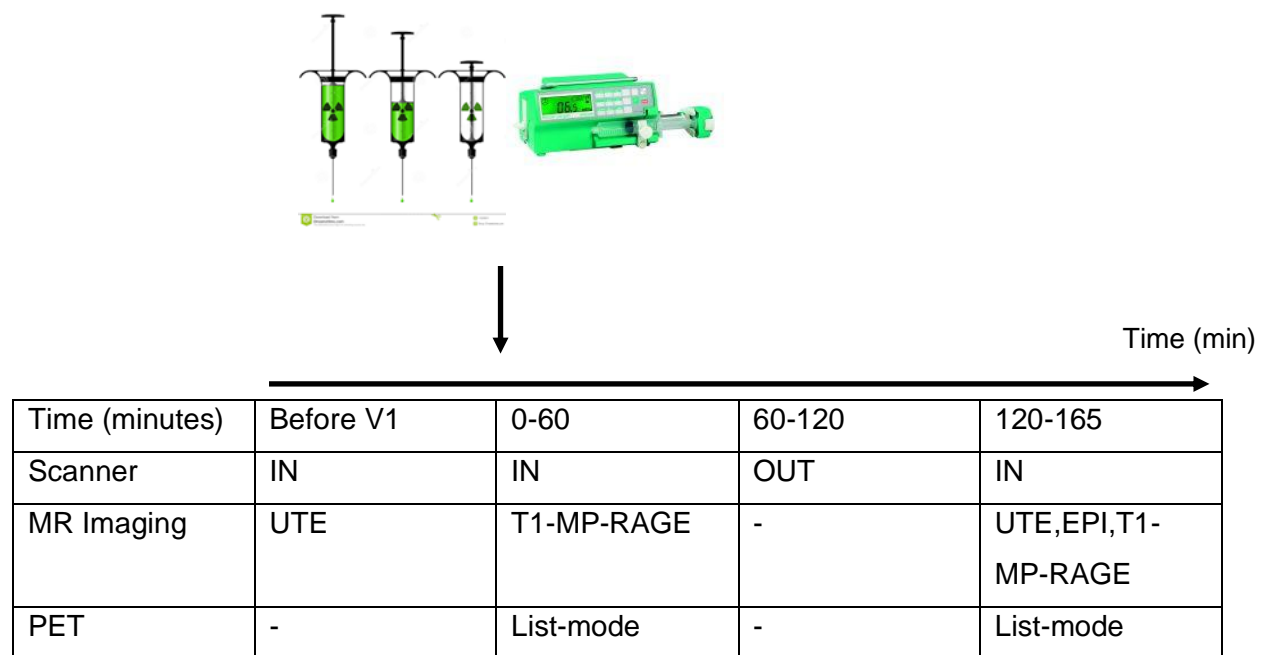
Figure 24: Baseline Examination

Abbreviations: UTE: ultra short-time echo sequence for Attenuation Correction[88];
MP-RAGE: magnetization prepared rapid gradient echo; EPI: echo-planar imaging

Figure 25: PET/MR Imaging Examination: (-)-[^{18}F]flubatine Bolus Application

Visit 2: Visual Food Cue Stimulation (V2)

The whole visual stimulation task lasted 14.2 minutes, starting at 120 minutes p.i. when equilibrium was reached. A beamer projected the food items onto a screen at the back of the scanner. Placing a mirror onto the MR imaging head coil in front of the face, the participants were able to look at the displayed visual food cues (n= 80 items). During the stimulation scan, a standard set of salient food cues were presented in a randomized block design.

Each visual food cue was displayed for 3 seconds. After every presented item, the individuals had 1.9 seconds to rate the previously shown cue: being able to choose between four buttons in a single-piece apparatus in their hands, participants were asked to answer on a 4-point Likert scale ranging from very much ("sehr") to not at all ("gar nicht") how much they want to eat the presented food item at that certain moment (see Figure 27). Jitter between rating process and following presented item lasted between 1.8 and 7.8 seconds. Scan ended at 165 minutes post injection.

Time (min)

Time (minutes)	Before V2	0-60	60-120	120-165
Scanner	IN	IN	OUT	IN
MR imaging	UTE	T1-MP-RAGE	-	Visual stimulus: UTE,EPI,T1-MP-RAGE
PET	-	List-mode	-	List-mode
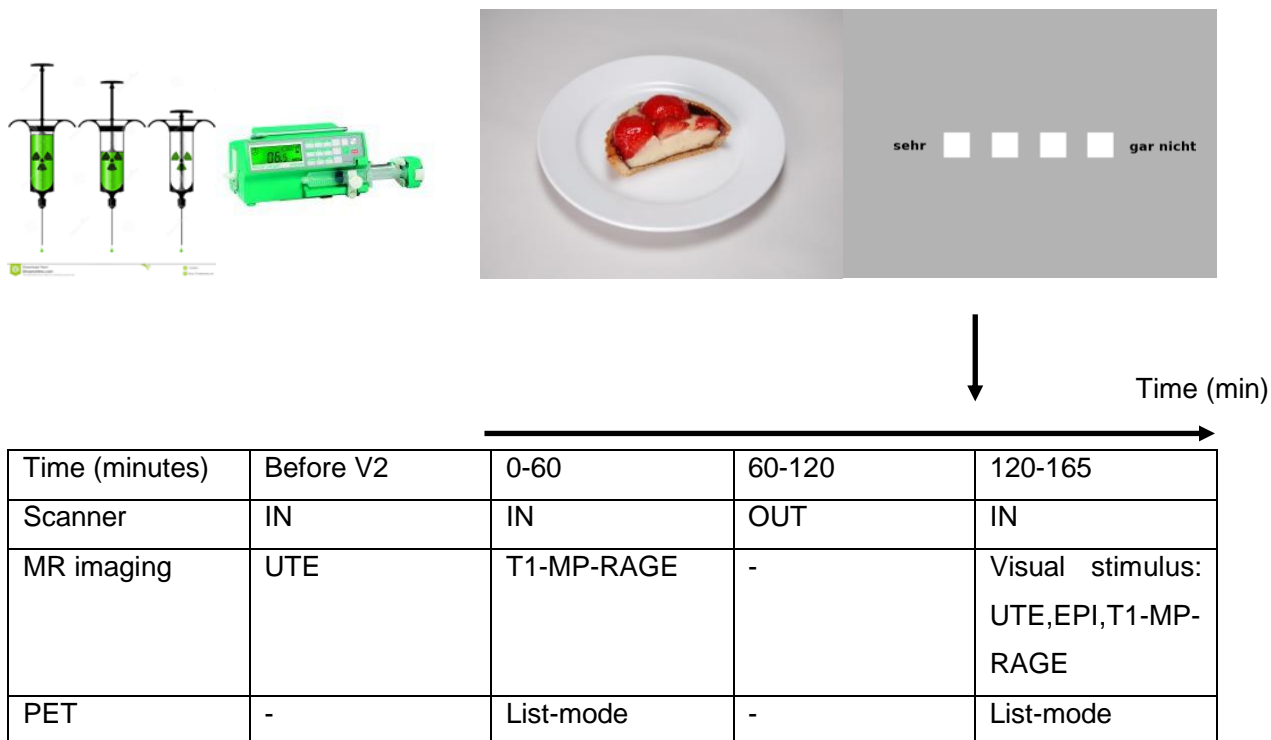
Figure 26: Stimulus Examination

Abbreviations: UTE: ultra short-time echo sequence for Attenuation Correction[88];

MP-RAGE: magnetization prepared rapid gradient echo; EPI: echo-planar imaging

Visit 3: Telephone Follow-up (V3)

Approximately two weeks after V2, a telephone follow-up was conducted in order to control for any (severe) adverse events, changes in concurrent medication or concomitant diseases.

6.6 Imaging Data and Blood Plasma Analysis

Co-registration and motion-correction procedures of PET and MR imaging data were performed using SPM2-software (*Statistical Parametrical Mapping, Wellcome Trust Centre for Neuroimaging, University College London, UK*). VOIs in five consecutive transversal brain slices were manually drawn using PMOD software (*PMOD Technologies Ltd., Zurich, Switzerland)*. Left and right VOIs (Figure 28, following page) of each hemisphere were later summed to their mean value to conduct statistical analyses (6.7 Statistical Analyses). Venous blood sampling was obtained for the calculation of our primary outcome measure V_T at 90, 105, 120, 135, 150, 165 minutes p.i. (Figure 27). This was based on the 120-165 minutes p.i. tracer concentration in tissue (C_{tissue}) at equilibrium divided by total radioactivity concentration in venous blood plasma (C_{plasma}), according to Innis et al..[62] Each sampling included 4 serum tubes which contained 2 ml, adding up to a total of 48 ml. Figure 27 depicts a TAC of one healthy volunteer in the NAc.
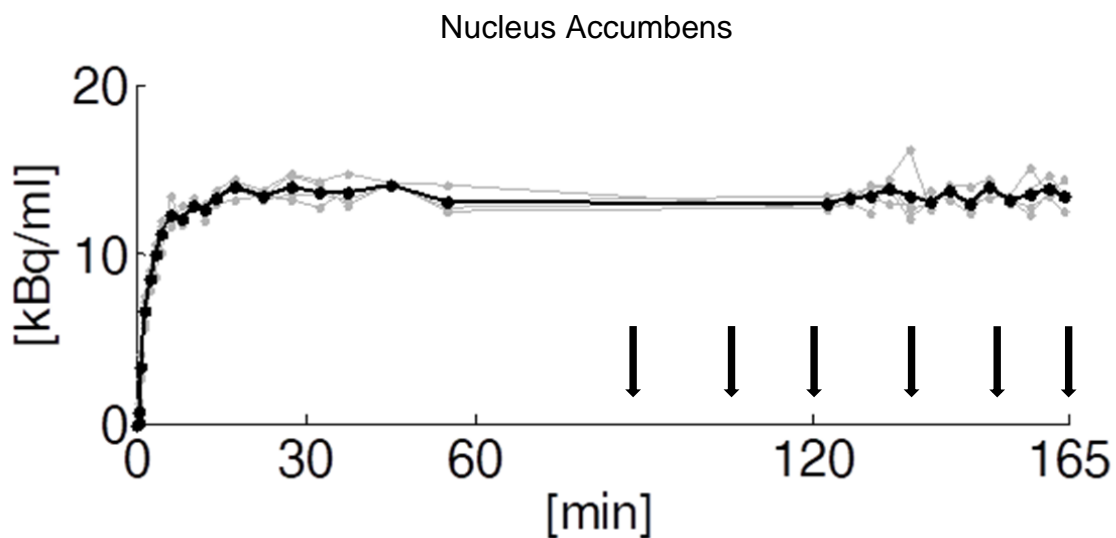
Nucleus Accumbens

Figure 27: TAC of One Healthy NW Volunteer

Equilibrium is reached after latest 120 min p.i with bolus-infusion protocol in nucleus accumbens, according to Hillmer et al.[75]. Schematic time frame of venous blood sampling for V_T calculation at 90, 105, 120, 135, 150 and 165 min p.i.
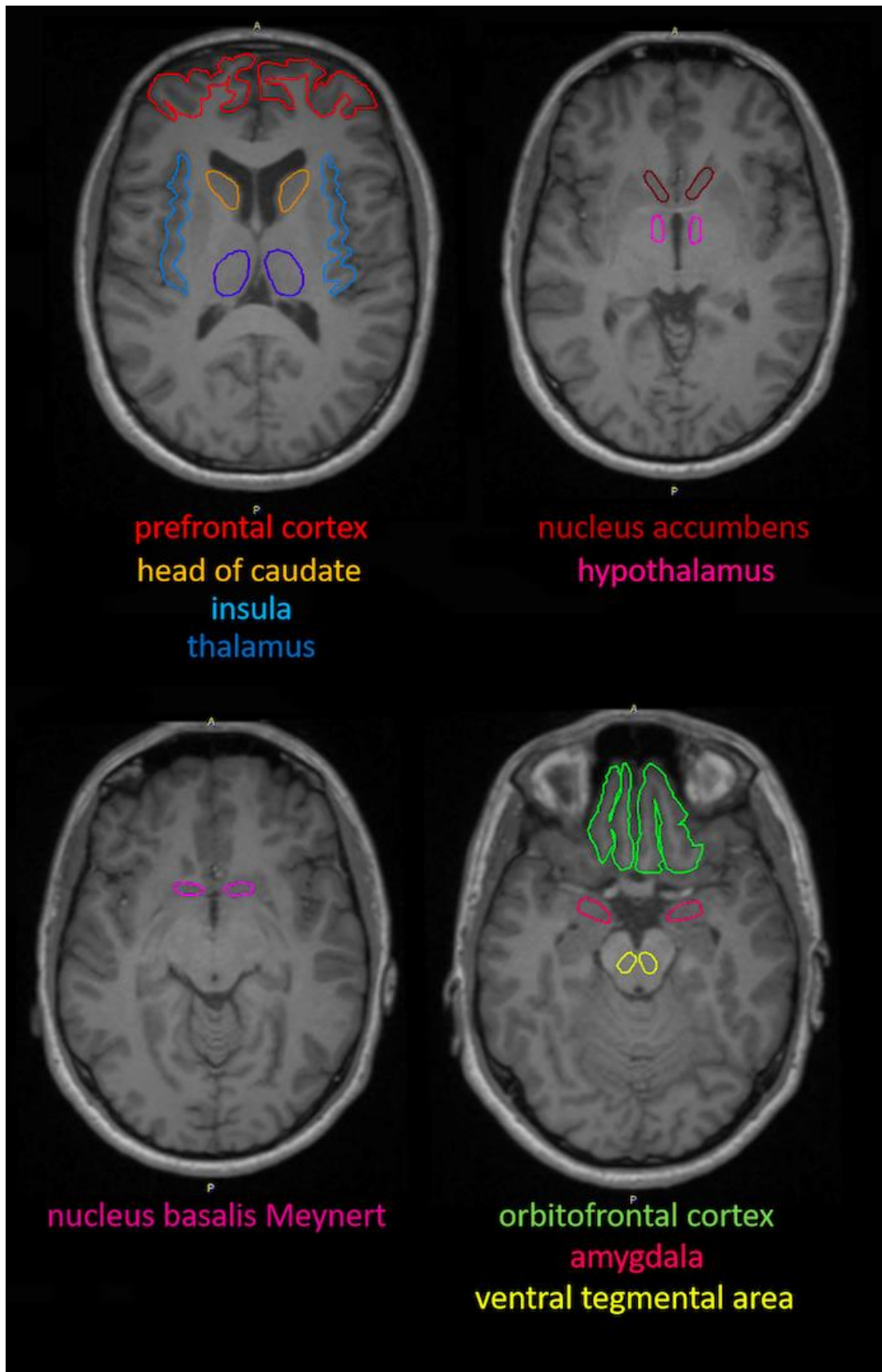
Figure 28: Volumes of Interest (VOI) of Preselected Brain Regions That Play a Crucial Role in Cholinergic Signaling

6.7 Statistical Analysis

Data analyses were carried out using *jamovi* (version 1.6, open source computer software). Applied Q-Q plots of our data showed distinct variation from normal distribution in some of our analyzed VOIs, making the follow-up Levene and Shapiro-Wilk tests to check for normal distribution and equality of variance redundant.

We therefore used non-parametrical Mann-Whitney-U test (MW-U) and to compare demographic parameters such as BMI, body weight, age as well as (-)-[^{18}F]flubatine application dosage between normal weight and obese study group. We also used Fisher's Exact test to compare the gender of our two study groups. To evaluate V_T differences in each VOI we conducted ANCOVA (Analysis of Covariance) correcting for age (covariate age $p < 0.05$ between NW and OB). Intra-individual differences between rest and stimulus conditions were assessed using the non-parametrical Wilcoxon dependent samples analysis. To investigate the relationship between VAS scores and α4β2 nAChR availability at resting state and stimulus conditions we applied Spearman rank correlation analyses. We also correlated changes between baseline and stimulus conditions via spearman rank correlation coefficients matrix of α4β2 nAChR availability and VAS scores.

7. Results

7.1 Epidemiological Data

Table 3 shows demographics as well as applied radiotracer concentrations. Dropouts occurred due to dizziness, nausea or canceling of visits of our study participants.

Table 3: Demographics

	Normal weight	Obese	p value
Participants	N=14	N=16	
Male / Female	3/11	6/10	0.44[a]
Without Baseline	-	2	
Without Stimulus	1	-	
Completed Baseline+Stimulus	13	14	
Age (years)			
Mean±SD	28.1±7.58	40.6±14.0	**0.002[b]**
Min-Max	19-45	20-62	
Weight (kg)			
Mean±SD	64.6±7.89	113±10.2	**<0.001[b]**
Min-Max	54-83	94-140	
BMI (kg/m^2)			
Mean±SD	21.8±1.90	37.8±3.18	**<0.001[b]**
Min-Max	18.7-24.9	32.5-42.8	
(-)-[^{18}F]flubatine (MBq); Visit 1			
Mean±SD	295±8.07	287±21.4	**0.03[b]**
Min-Max	273-308	207-301	
(-)-[^{18}F]flubatine (MBq); Visit 2			
Mean±SD	292±8.18	298±5.48	0.23[b]
Min-Max	276-307	283-300	

[a] Fisher Exact test; [b] non-parametrical MW-U; BMI: body mass index; SD: standard deviation; Min: Minimum; Max: Maximum; MBq: Megabecquerel

7.2 Baseline and Stimulus V_T Calculations

To evaluate V_T differences in each VOI between NW and OB, we conducted ANCOVA correcting for age in both baseline and stimulus conditions. Table 4 and Figure 29 indicate the data distribution and statistics of calculated V_T under baseline conditions. OB tend to show lower V_T in the NBM and higher V_T in the thalamus although, overall, no statistically significant differences in V_T between our two groups under baseline conditions were found.

Baseline Scan (Visit 1)

Table 4: Distribution Volumes (V_T) in NW and OB Under Baseline Conditions (ANCOVA Correcting for Age)

Baseline (Visit 1)	Mean V_T NW	Mean V_T OB	Mean difference	p value	Effect Size (η_p^2)
Amygdala	8.85	9.08	-0.229	0.607	0.010
HPT	13.2	13.3	-0.141	0.864	0.001
Insula	9.34	9.71	-0.369	0.673	0.023
NAc	10.3	10.6	-0.243	0.657	0.007
Nc. Caud.	10.1	10.4	-0.225	0.661	0.007
OFC	8.68	9.04	´-0.366	0.437	0.022
PFC	8.64	9.06	-0.421	0.383	0.027
Thalamus	25.5	27.7	-2.26	0.116	0.086
VTA	17.2	16.6	0.638	0.486	0.017
NBM	11.6	10.2	1.35	0.119	0.084

Abbreviations: HPT – Hypothalamus; NAc – Nucleus Accumbens; Nc. Caud. – Nucleus Caudatus; OFC – Orbitofrontal Cortex; PFC – Prefrontal Cortex; VTA – Ventral Tegmental Area; NBM – Nucleus Basalis of Meynert

Amygdala

HPT

p= 0.607

p= 0.864

Insula

NAc

p= 0.673

p= 0.657

Nc. Caud.

OFC

p= 0.661

p= 0.437

48
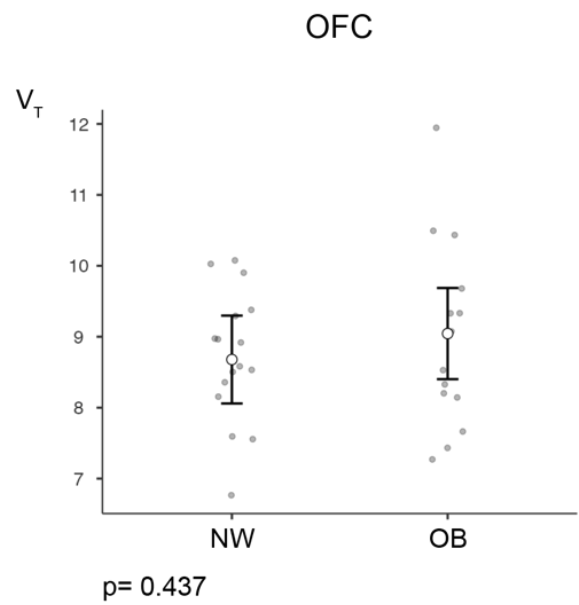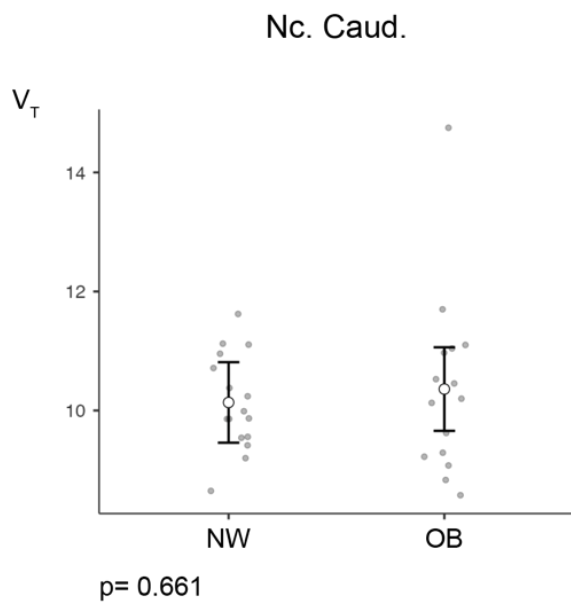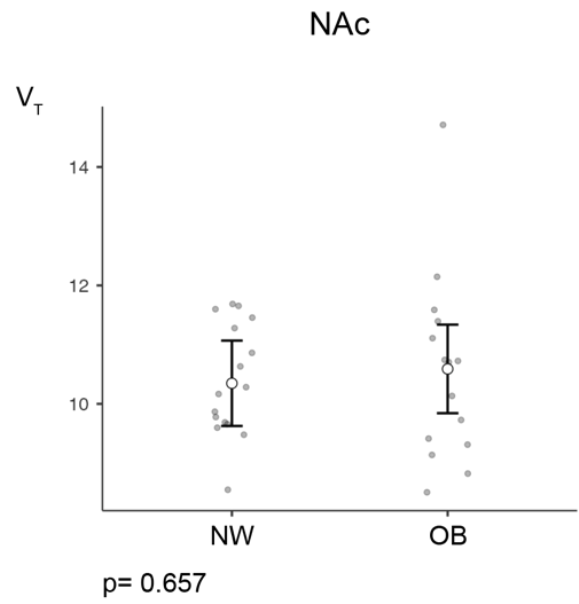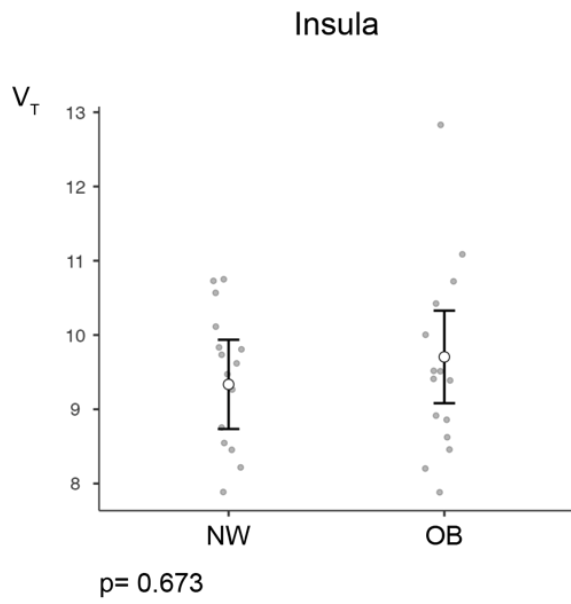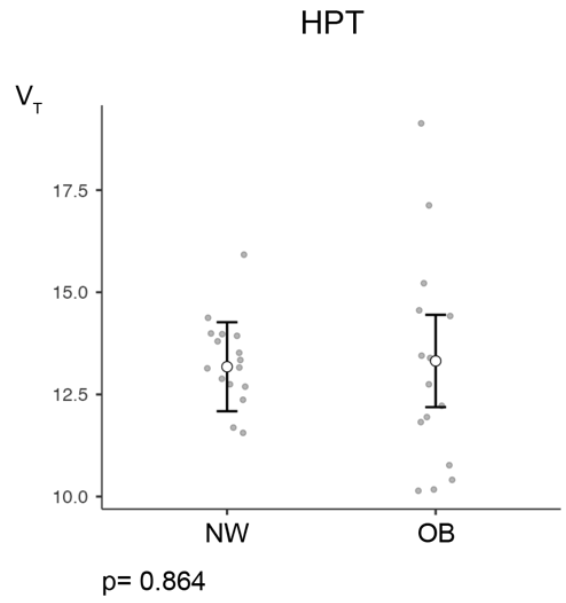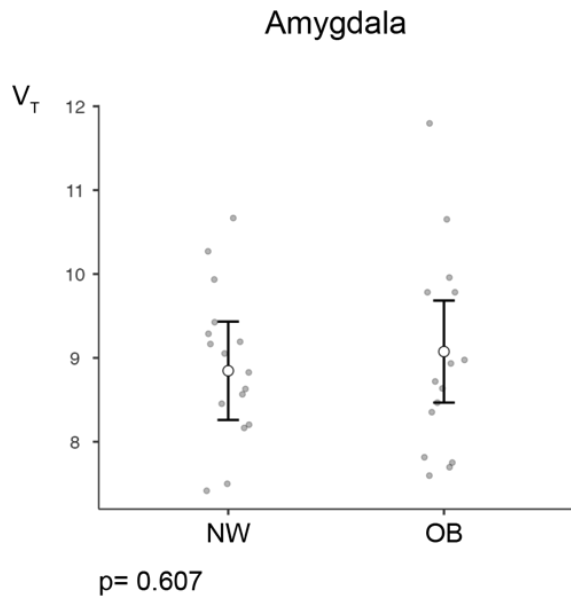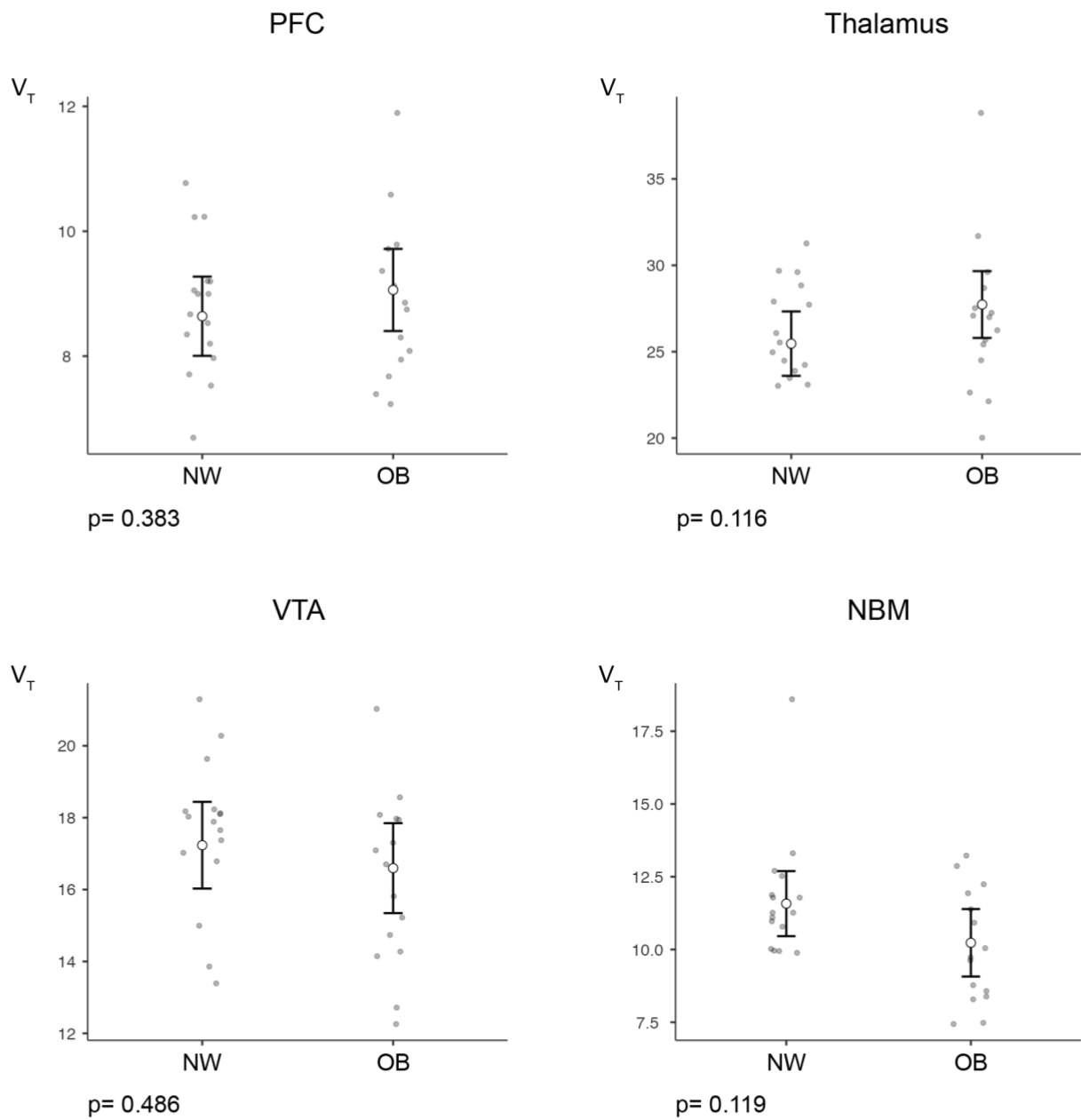
Figure 29: Mean V_T in NW and OB: Baseline Scan

x axis: NW: normal weight; OB: obesity; y axis: V_T (mean)

jitter plots indicating observed mean scores; bars representing confidence intervals

After correcting for age (ANCOVA), OB participants showed higher V_T in thalamic VOI (p=0.028; $\eta^2 p=0.167$). No statistically significant differences in V_T in other brain regions were found (Table 5, Figure 30).

Table 5: Distribution Volumes (V_T) in NW and OB Under Stimulus Conditions
(ANCOVA Correcting for Age)

Stimulation (Visit 2)	Mean V_T NW	Mean V_T OB	Mean difference	p value	Effect Size (η_p^2)
Amygdala	8.88	9.13	-0.255	0.573	0.012
HPT	13.3	13.7	-0.424	0.623	0.009
Insula	9.30	9.91	-0.608	0.194	0.062
NAc	10.3	10.8	*-0.489*	0.378	0.029
Nc. Caud.	10.2	10.6	*-0.460*	0.416	0.025
OFC	8.67	9.22	*-0.550*	0.252	0.048
PFC	8.63	9.18	*-0.548*	0.248	0.049
Thalamus	**25.1**	**28.8**	***-3.63***	**0.028**	**0.167**
VTA	17.3	17.0	*0.298*	0.769	0.003
NBM	11.1	10.5	*0.628*	0.336	0.034

Abbreviations: HPT – Hypothalamus; NAc – Nucleus Accumbens; Nc. Caud. – Nucleus Caudatus; OFC – Orbitofrontal Cortex; PFC – Prefrontal Cortex; VTA – Ventral Tegmental Area; NBM – Nucleus Basalis of Meynert

Amygdala

p= 0.573

HPT

p= 0.623

Insula

V_T

NW   OB

p= 0.194

NAc

V_T

NW   OB

p= 0.378

Nc. Caud.

V_T

NW   OB

p= 0.416

OFC

V_T

NW   OB

p= 0.252

PFC

V_T

NW   OB

p= 0.248

Thalamus

V_T

NW   OB

p= 0.028
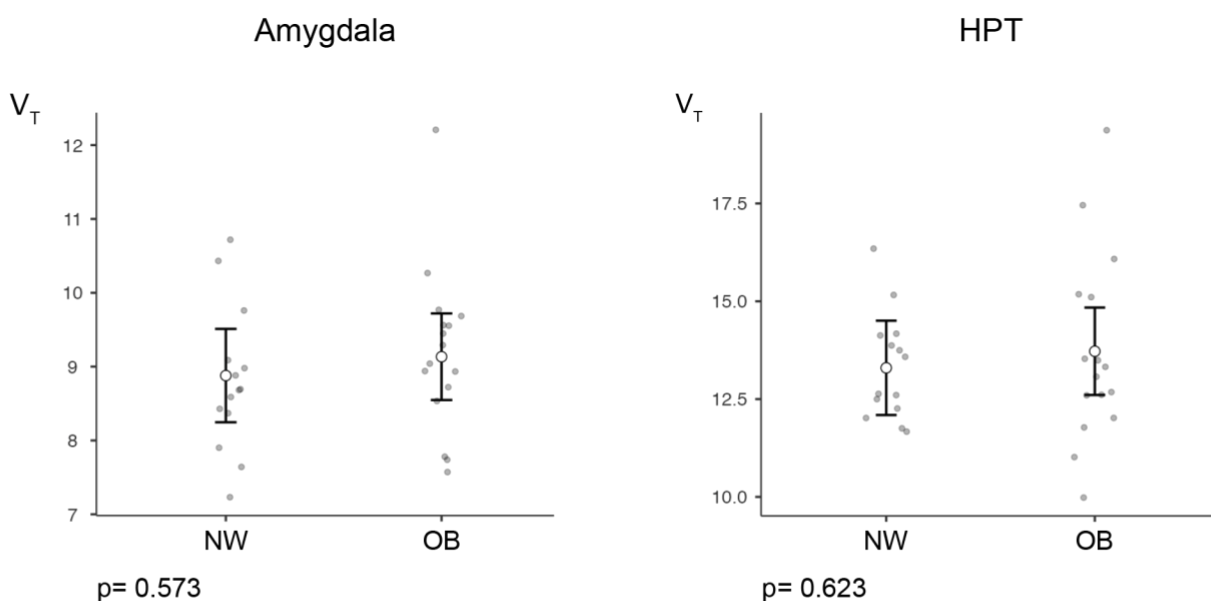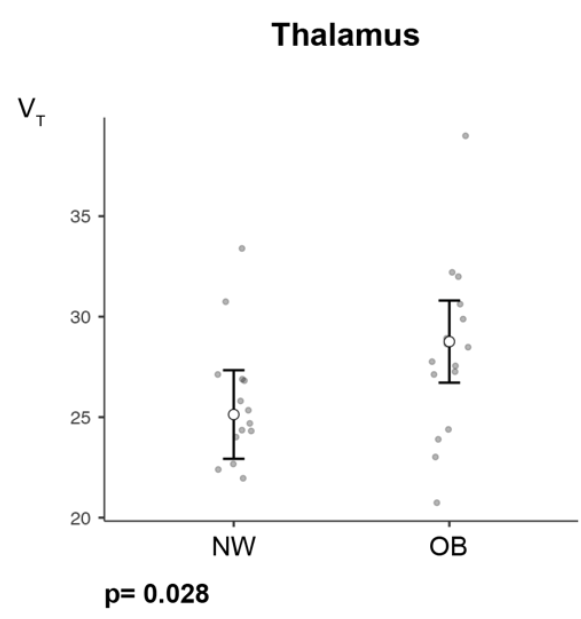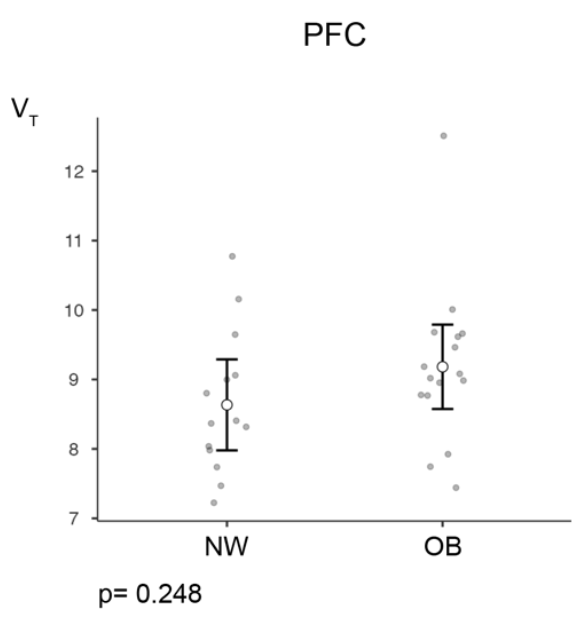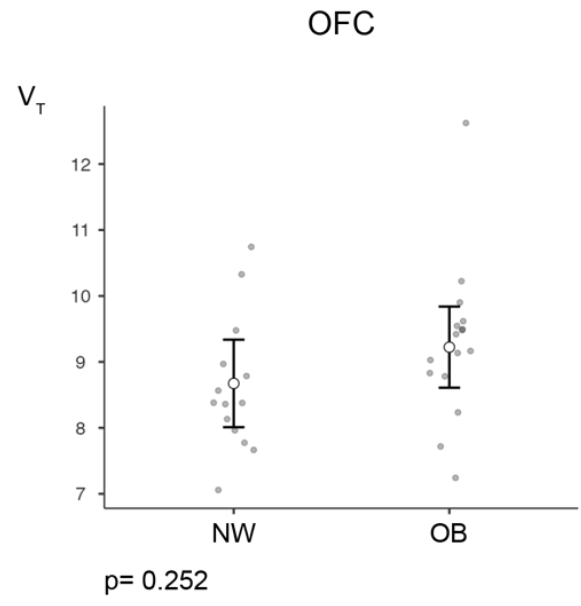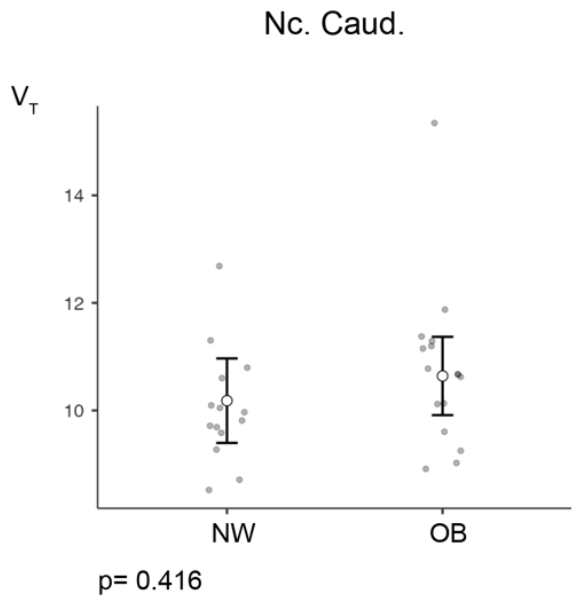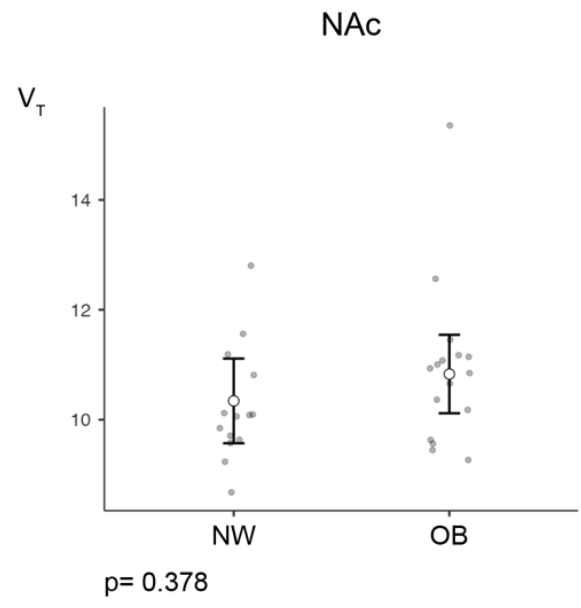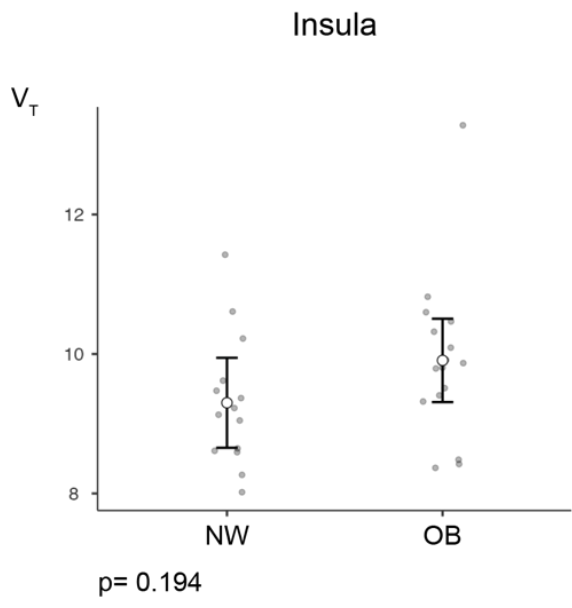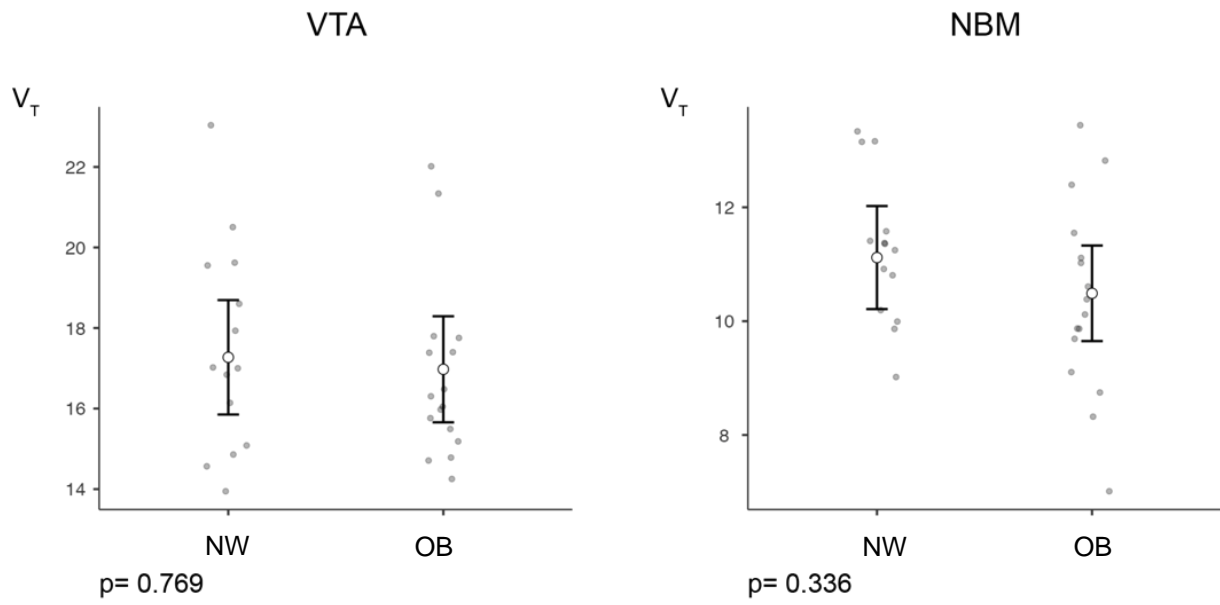
Figure 30: Mean V_T in NW and OB: Stimulus Scan

x axis: NW: normal weight; OB: obesity; y axis: V_T (mean)

jitter plots indicating observed scores; bars representing confidence intervals

7.3 Intra-individual V_T Assessment Between Baseline and Stimulus Conditions

We intra-individually assessed differences in V_T in a paired samples analysis in each study group between baseline and stimulus conditions, looking for changes in V_T that are caused by the presentation of visual food cues. In both paired samples analyses (comparison NW and OB: baseline and stimulus scan, respectively) no statistically significant differences in V_T were found (Table 6, Table 7). However, OB showed greater intra-individual mean differences in V_T between resting state and stimulus conditions (Figure 31) and a tendency to smaller p values compared with NW (e.g. VTA NW: mean difference 0.02, p=1.00; OB: mean difference -0.686; p=0.11)

Table 6: Baseline Versus Stimulus V_T Assessment in _NW_ Participants

VOIs (NW)	Baseline; mean V_T	Stimulus; mean V_T	Mean difference	p value	Effect size
Amygdala	8.81	8.81	0.01	1.00	0.01
HPT	13.30	13.2	-0.06	0.81	-0.09
Insula	9.34	9.30	0.002	1.00	0.01
NAc	10.26	10.24	-0.02	0.90	-0.05
Nc. Caud.	10.05	10.06	-0.04	0.86	-0.07
OFC	8.62	8.61	-0.03	0.95	-0.03
PFC	8.61	8.64	-0.02	0.95	-0.03
Thalamus	26.03	25.75	0.21	0.90	0.05
VTA	17.46	17.48	0.02	1.00	0.01
NBM	11.68	11.24	0.18	0.46	0.24

Abbreviations: HPT – Hypothalamus; NAc – Nucleus Accumbens; Nc. Caud. – Nucleus Caudatus; OFC – Orbitofrontal Cortex; PFC – Prefrontal Cortex; VTA – Ventral Tegmental Area; NBM – Nucleus Basalis of Meynert

Table 7: Baseline Versus Stimulus V_T Assessment in _OB_ Participants

VOIs (OB)	Baseline; mean V_T	Stimulus; mean V_T	Mean difference	p value	Effect size
Amygdala	8.98	9.26	-0.286	0.24	-0.39
HPT	13.49	13.81	-0.305	0.19	-0.43
Insula	9.57	9.96	-0.397	0.19	-0.43
NAc	10.62	10.90	-0.276	0.38	-0.30
Nc. Caud.	10.42	10.82	-0.351	0.24	-0.39
OFC	9.02	9.32	-0.263	0.31	-0.34
PFC	8.90	9.23	-0.368	0.22	-0.41
Thalamus	26.70	28.42	-1.418	0.15	-0.47
VTA	15.95	16.73	-0.686	0.11	-0.52
NBM	9.99	10.40	-0.463	0.24	-0.39

Abbreviations: HPT – Hypothalamus; NAc – Nucleus Accumbens; Nc. Caud. – Nucleus Caudatus; OFC – Orbitofrontal Cortex; PFC – Prefrontal Cortex; VTA – Ventral Tegmental Area; NBM – Nucleus Basalis of Meynert

Figure 31 and Figure 32 demonstrate the greater V_T mean difference and smaller p values in OB between resting state and stimulus conditions compared with NW.

Thalamus

p= 0.90 / mean difference= 0.21

p= 0.15 / mean difference= -1.42
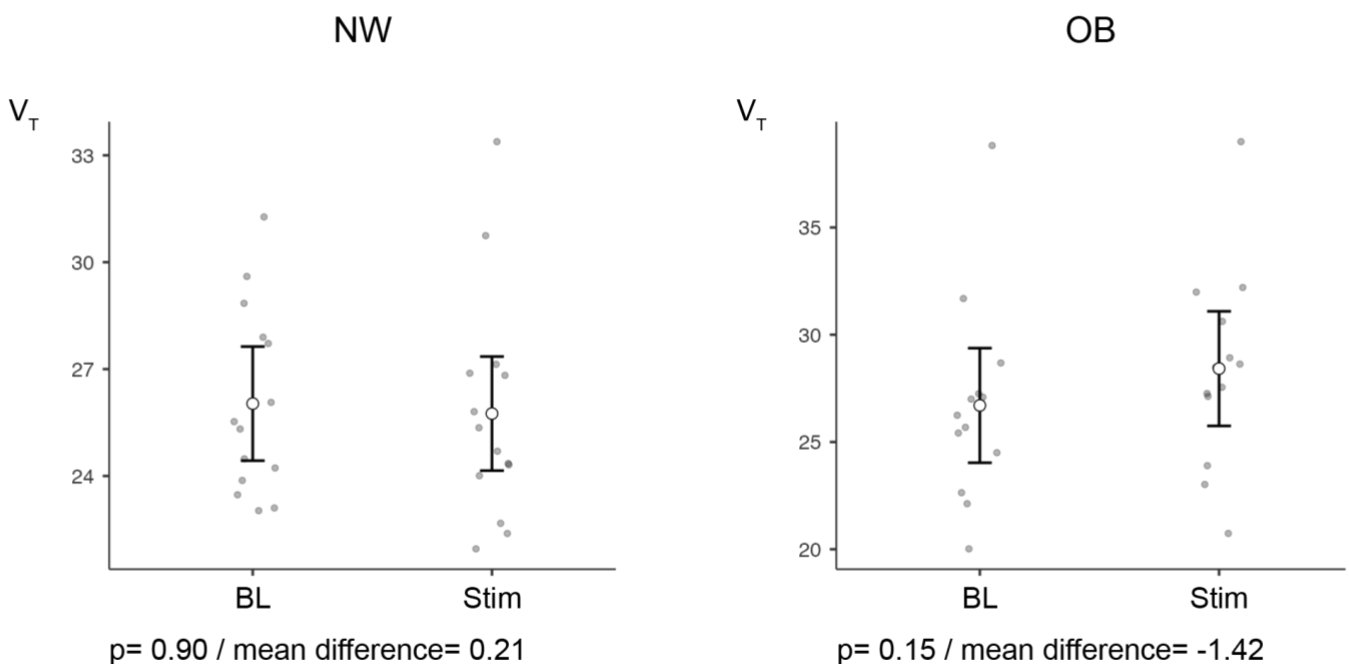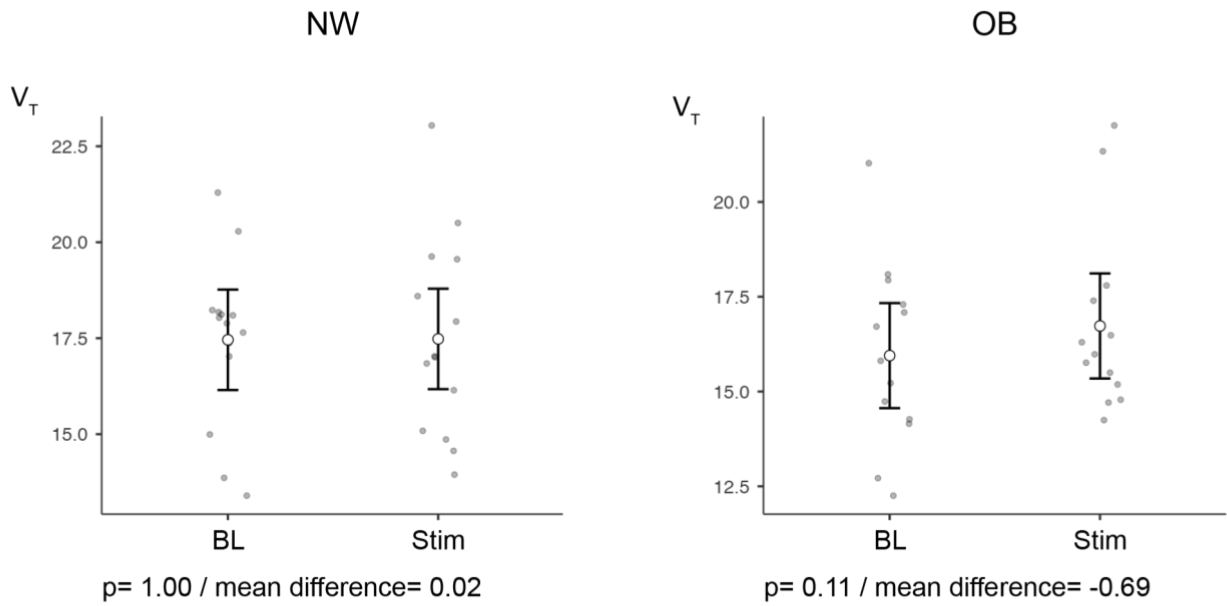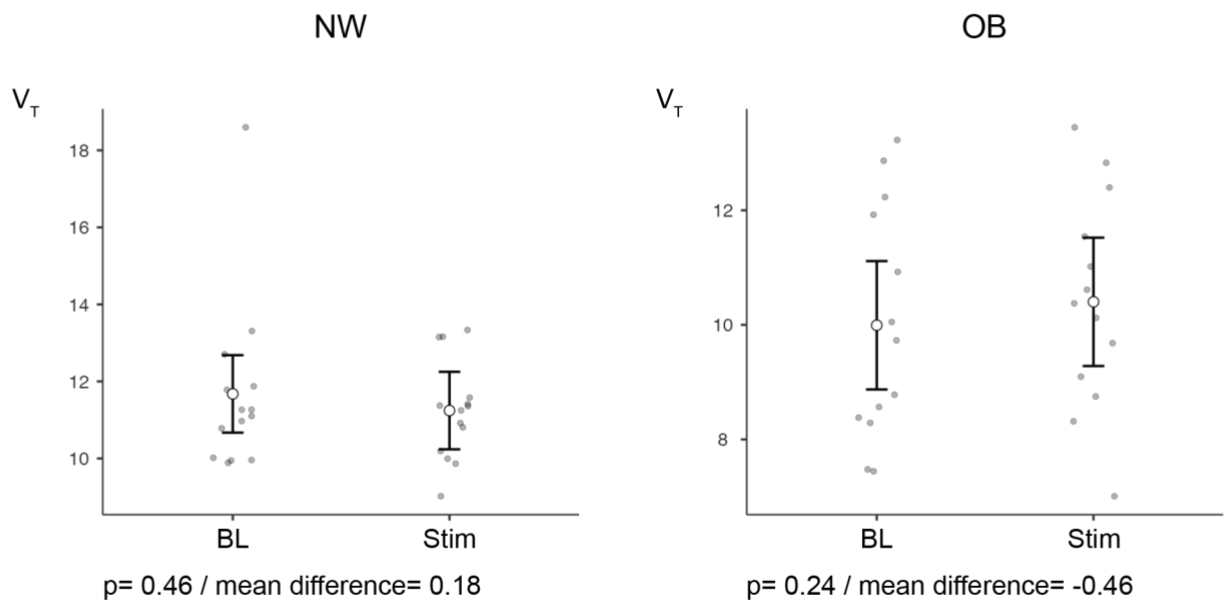
Figure 31: Intra-individual V_T Between Baseline and Stimulus Conditions

x axis: BL: baseline examination; Stim: stimulus examination; y axis: V_T (mean)

Abbreviations: VTA – Ventral Tegmental Area; NBM – Nucleus basalis of Meynert
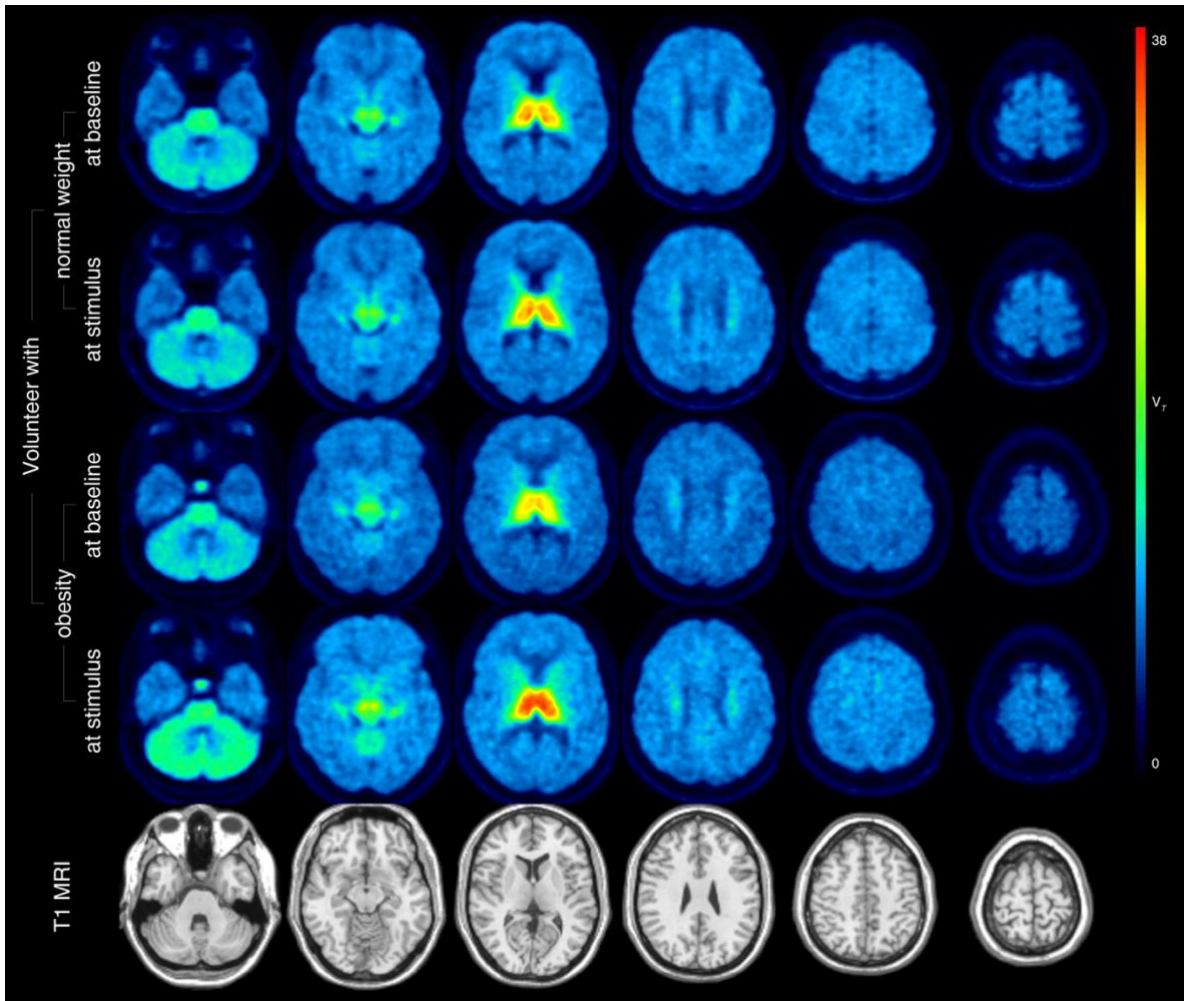
Figure 32: Baseline Versus Stimulus Assessment

Distribution volume (V_T) of (-)-[^{18}F]flubatine in one OB and one NW at baseline and under stimulus conditions. Note the increase in thalamic V_T in OB between baseline and stimulus while V_T was stable in NW.

First row: NW at baseline; Second row: NW at stimulus; Third row: OB at baseline; Fourth row: OB at stimulus; Fifth row: T1-MR imaging data

7.4 Correlational Analyses of VAS Versus V_T

Figure 33 shows the correlation between regional V_T and obtained VAS scores of NW. NW present statistically significant negative correlation coefficients between VAS Score "craving" and several VOIs such as VTA (r= -0.61), NAc (r= -0.58), OFC (r= -0.52), and insula (r= -0.55) as well as thalamus (r= -0.74). Interestingly, these significant negative correlations seem to disappear under stimulus conditions.
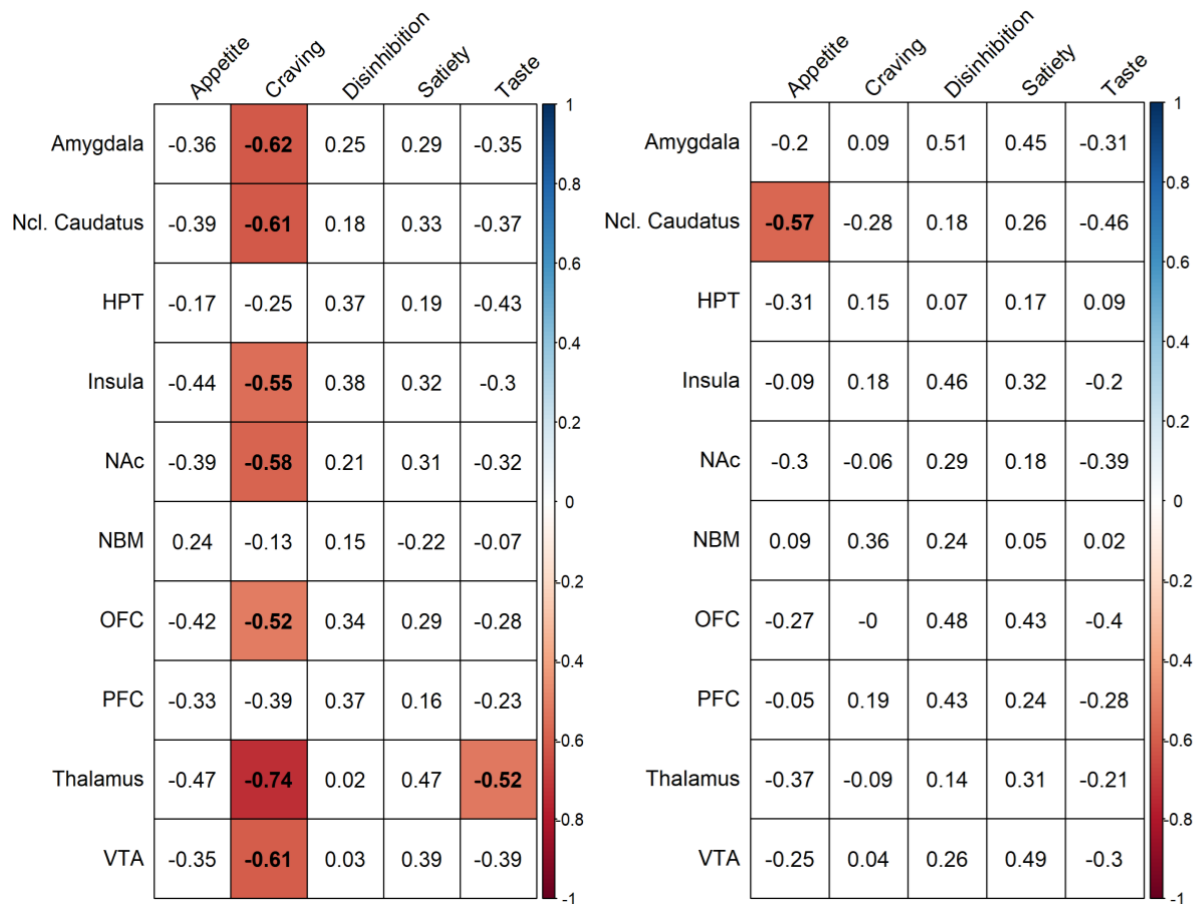
Figure 33: Spearman Rank Correlation Coefficients Matrix in NW

Relationship of V_T in different VOIs and VAS under baseline (left) and stimulus conditions (right). Significant (p<0.05) correlations marked as blue (positive) or red (negative).

Abbreviations: Ncl. Caudatus – Nucleus caudatus; HPT – Hypothalamus; - NAc – Nucleus accumbens; NBM – Nucleus basalis of Meynert; OFC – Orbitofrontal Cortex; PFC – Prefrontal Cortex; VTA – Ventral Tegmental Area

Figure 34 depicts the correlation between V_T and VAS scores of OB. This analysis revealed a statistically significant negative correlation between VAS Score "disinhibition" and distinct VOIs such as NBM (r= -0.54), thalamus (r= -0.64),

VTA (r= -0.58), NAc (r= -0.56), OFC (r= -0.52), PFC (r= -0.59). No further significant correlations under stimulus conditions were found. Figure 35 and Figure 36 highlight group-specific differences in correlational analyses.
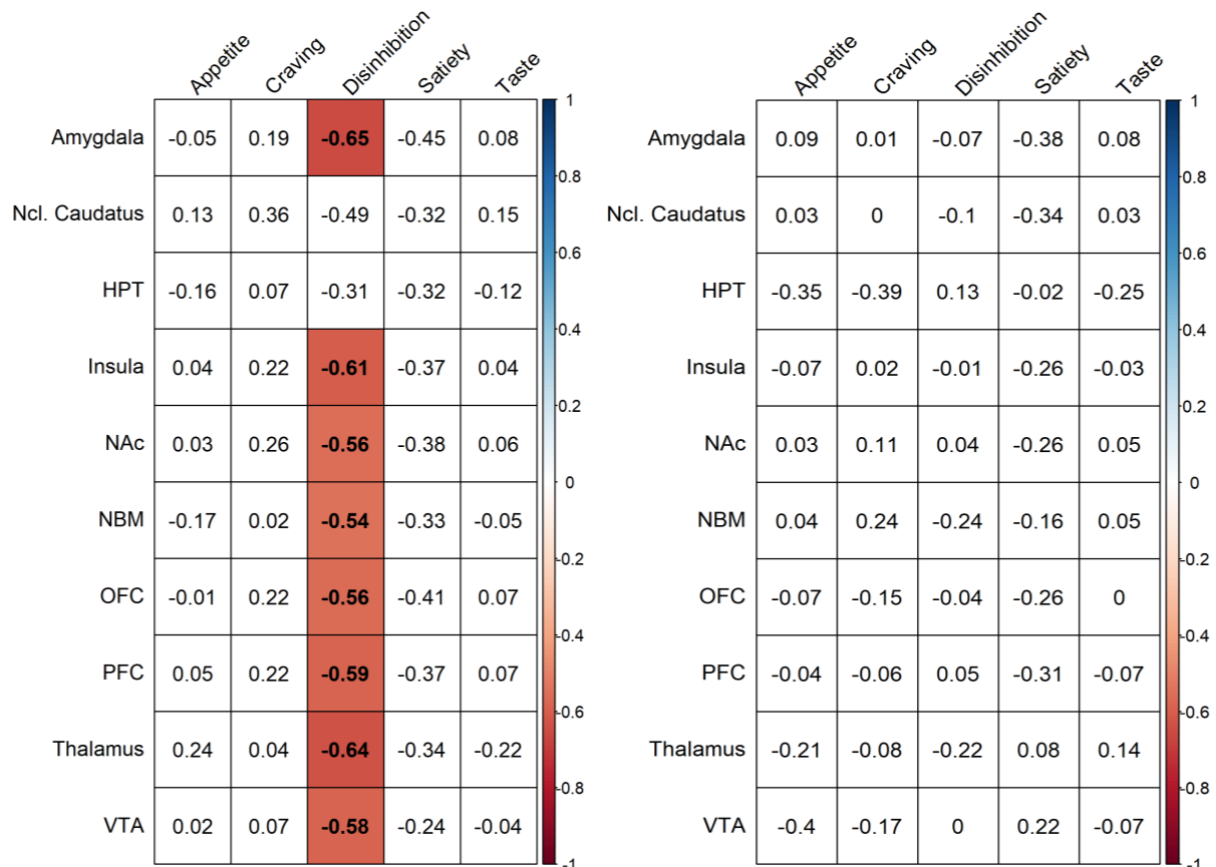
Figure 34: Spearman Rank Correlation Coefficients Matrix in OB

Relationship of V_T in different VOIs and VAS under baseline (left) and stimulus conditions (right). Significant (p<0.05) correlations marked as blue (positive) or red (negative).

Abbreviations: Ncl. Caudatus – Nucleus caudatus; HPT – Hypothalamus; - NAc – Nucleus accumbens; NBM – Nucleus basalis of Meynert; OFC – Orbitofrontal Cortex; PFC – Prefrontal Cortex; VTA – Ventral Tegmental Area

NW Correlational Analyses - Scatterplots

Thalamus (V_T)
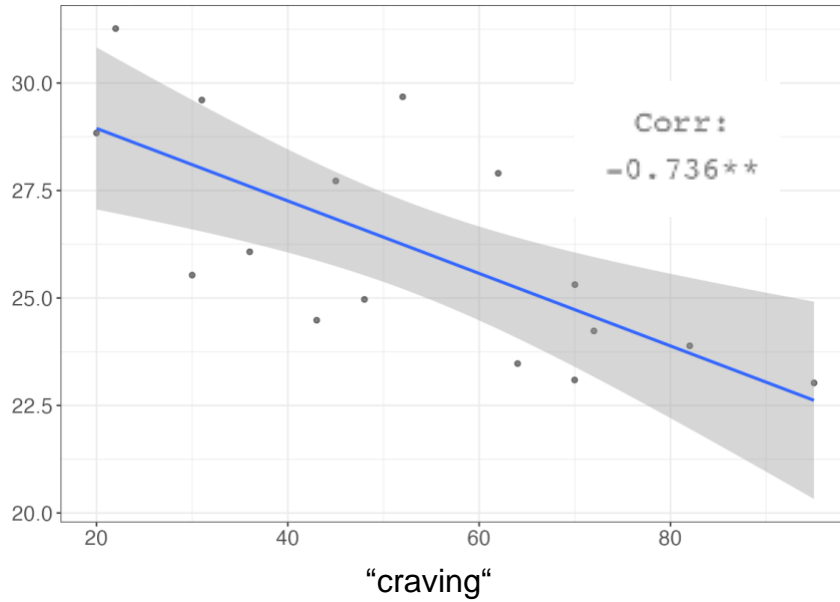
Baseline

Thalamus (V_T)

Stimulus

Note. * $p < .05$, ** $p < .01$, *** $p < .001$

Figure 35: Scatterplot of NW Thalamic V_T and VAS "craving"

Including regression line with 95 % confidence interval

(when significantly correlated)

Data of NW participants under baseline (**p< 0.05; r= -0.74**) and stimulus (p> 0.05; r= -0.09)

conditions; r= correlation coefficient (Corr)

OB Correlational Analyses - Scatterplots

Thalamus (V_T)

Baseline

Corr:
−0.637*

"disinhibition"

Thalamus (V_T)

Stimulus

Corr:
−0.224

"disinhibition"

Note. * p < .05, ** p < .01, *** p < .001

Figure 36: Scatterplot of Thalamic V_T and VAS "disinhibition"

Including regression line with 95 % confidence interval

(when significantly correlated)

Data of OB participants under baseline (**p<0.05; r= -0.64**) and stimulus

(p>0.05; r= -0.22) conditions; r= correlation coefficient (Corr)

Figure 37 and Figure 38 illustrate the relationship between the correlation of changes in V_T and changes in VAS scores between baseline and stimulus conditions. Here, NW demonstrate a significant positive correlation between the HPT and "satiety" (r= 0.61), which is significantly different from the same relationship in OB (p= 0.009). OB show a significant negative correlation between NAc and "disinhibition" (r= -0.59), whereas this relationship compared to NW almost reaches statistical significance (p= 0.082).
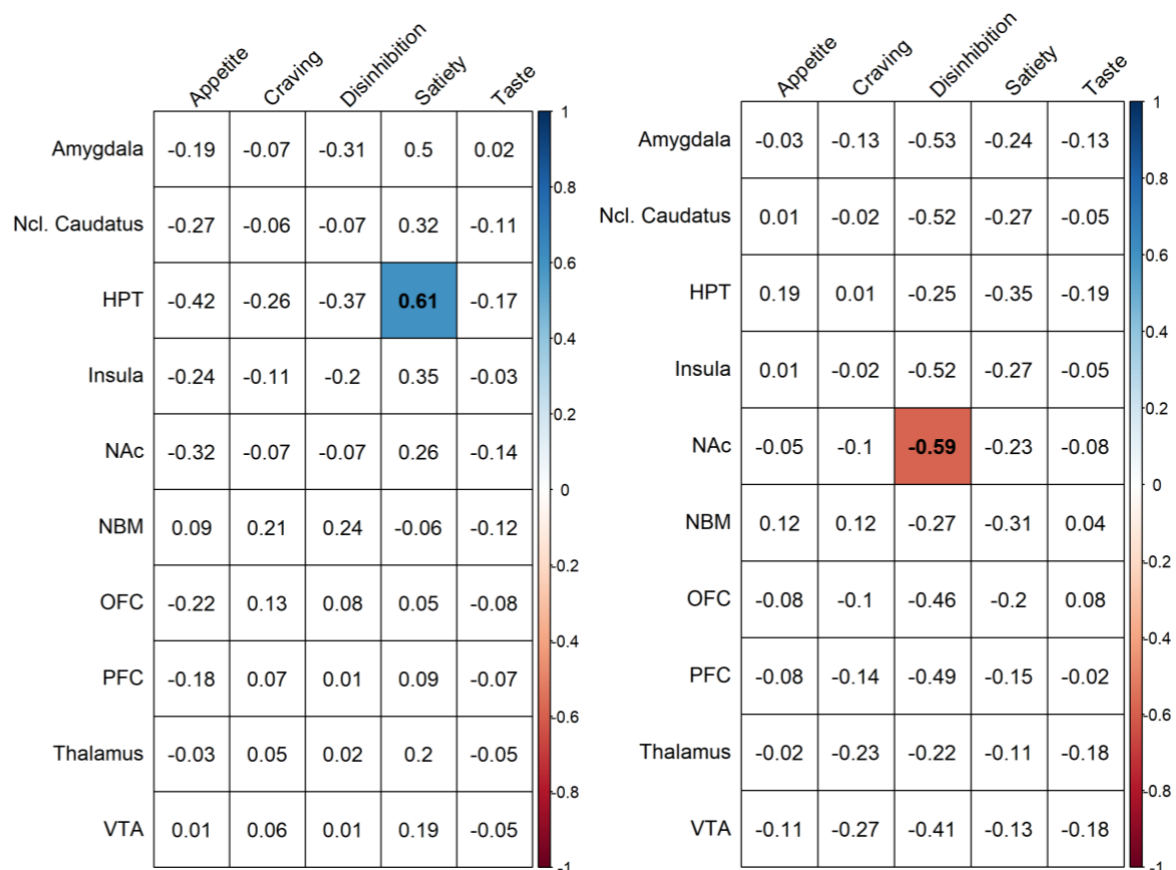
Figure 37: Correlation of Changes Between Baseline and Stimulus Conditions via Spearman Rank Correlation Coefficients Matrix of Distribution Volume V_T and VAS
(correlation coefficient r per VOI; mean V_T Stimulus – mean V_T Baseline)
and VAS scores (mean VAS Stimulus - mean VAS Baseline)
of NW (left) and OB (right) study participants.
Significant (p<0.05) correlations marked as blue (positive) or red (negative)

Abbreviations: Ncl. Caudatus – Nucleus caudatus; HPT – Hypothalamus; - NAc – Nucleus accumbens; NBM – Nucleus basalis of Meynert; OFC – Orbitofrontal Cortex; PFC – Prefrontal Cortex; VTA – Ventral Tegmental Area
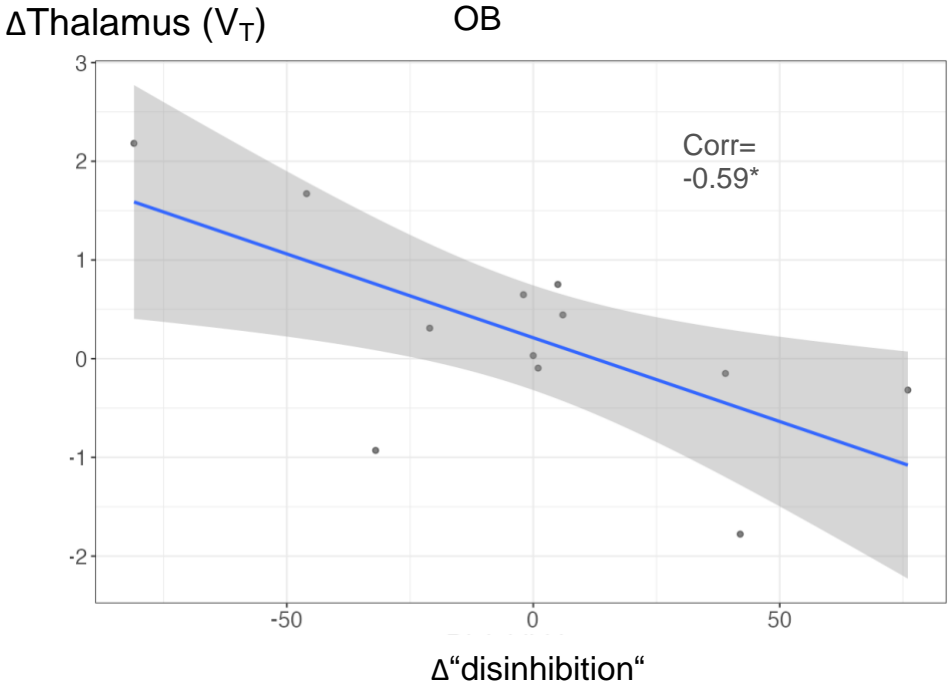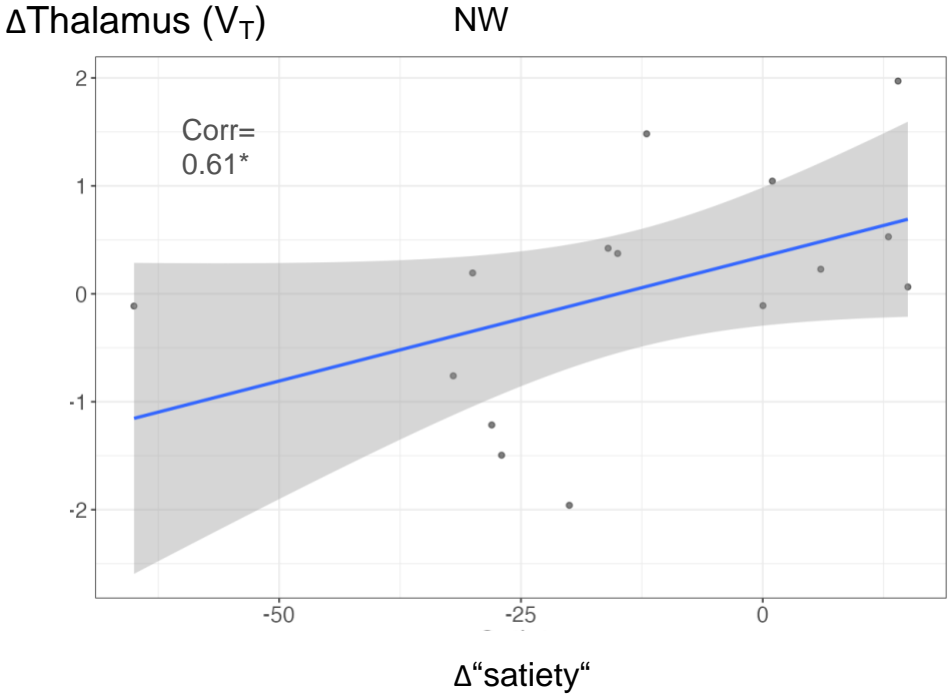
Figure 38: Correlation of Changes Between Baseline and Stimulus Conditions

V_T Stimulus – V_T Baseline correlated with VAS Stimulus – VAS Baseline

(both mean)

8. Discussion

This is a prospective, open, monocentric phase 0/I, proof-of-concept PET/MR imaging on cholinergic neuromodulation in obesity and its role in processing the effects of salient food stimuli. Dynamic PET data were obtained using the α4β2 nAChR specific radiotracer (-)-[^{18}F]flubatine. We specifically elucidated nAChR with (-)-[^{18}F]flubatine in an *in vivo* human baseline versus stimulus experimental design not only investigating resting state but also task-related cholinergic signaling in human obesity. Final outcome measures were differences in (-)-[^{18}F]flubatine V_T between NW and OB in resting state and stimulus conditions in unpaired as well as paired samples analyses. Secondary, we explored whether changes in eating behavior measured by VAS (visual analogue scores) are correlated with changes in α4β2 nAChR availability.

<u>Baseline V_T Calculations</u>

In an independent samples analysis we compared α4β2 nAChR availability between NW and OB under baseline conditions. Correcting for age, we did not find statistically significant differences in V_T between our two study groups. Yet, we did observe a tenden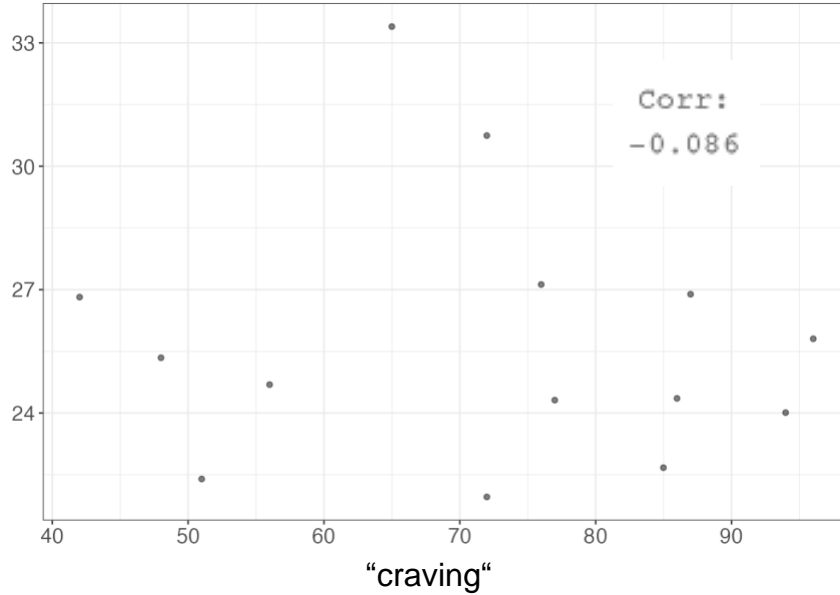cy to lower OB V_T in NBM compared with NW. The NBM is the central basal forebrain area of cholinergic transmission that innervates the amygdala as well as almost the entire cortical mantle.[26] Changes in nAChR availability in this region can therefore be assumed to affect widespread neuronal circuits computing sensory stimuli. Bentley et al.[89] describe neuronal network activation as a function of ACh levels which can be depicted in an inverted U-shape, similar to the Yerkes-Dodson law highlighting non-linear relationships between arousal, cognitive activation and task performance.[90] Thereby, Bentley et al. compared a so called relative hypocholinergic state to cigarette-deprived smokers and sufficient cholinergic tone to non-smokers. As mentioned above, overstimulation of nAChR can lead to receptor desensitization. Quick et al.[91] define the process of desensitization as a decrease or loss of biological response following prolonged or repetitive stimulation.

The tendency to lower baseline V_T of OB could potentially indicate a state of food stimuli deprivation during the scan represented by nAChR desensitization, similar to nicotine-deprived smokers. Contradicting this argument Graupner et al.[28] pointed out that nAChR have their highest affinity to its ligand while being desensitized. An interesting approach to disentangle this phenomenon would be to differ between fast-

onset and slow-onset desensitized receptor state in our study group, as both differ in their ligand affinity.[28] Limited temporal resolution of PET examinations however might not be able to detect changes in nAChR conformation as this happens in a millisecond to minutes timeframe versus temporal resolution in neuroreceptor PET ranging from 0.5 min – 10 min.[17,28,35]

Interestingly, Picciotto et al. pointed out that nicotinic stimulation of nAChR leads to a shift from tonic to phasic firing of DA neurons, potentially increasing the salience of sensory cues as inhibitory GABA release is rapidly decreased due to presynaptic nAChR desensitization.[35] These mesolimbic feedback loops affected by cholinergic neuromodulation could therefore enhance the detection of cues associated with reward, such as food.

Also, studies in rats showed that nAChR desensitization following nicotine exposure lead to a long lasting increase in reward sensitivity, which was mediated by nAChR upregulation.[54] As this increase in reward sensitivity could also be transferred to other substances of abuse, the sequence of cholinergic stimuli leading to desensitization and lastly nAChR upregulation to recover from desensitization, could explain a potential pathway to enter a state of "reward hyperexcitability".[54]

Simulating a state of nAChR desensitization through ablation of cholinergic neurons using a Cre-dependent14 adeno-associated virus (AAV) in the BF in rodents, lead to hyperphagia and substantial weight-gain compared to their control group.[57] Also, nicotinic stimulation of anorexigenic neurons in the hypothalamus induces satiety.[56] Mitigated cholinergic signaling of NBM in our OB study group, could therefore impair satiety pathways, eventually leading to prolonged appetite. Conversely, Dezfuli et al. showed that prolonged nAChR desensitization in mice through application of β2-selective agonist sazetidine-A (SAZ-A) lead to decreased body weight and food intake.[92] Lastly, the precise role of nAChR desensitization affecting eating behavior thus remains somewhat elusive.

Stimulus V_T Calculations

Our two-tailed independent samples analysis under stimulus conditions showed significantly higher α4β2 nAChR availability in the thalamus region in OB compared to NW. Correcting for age, these findings robustly endured ($p=0.028$; $\eta^2 p=0.167$). The thalamus plays a pivotal role in the processing of sensory information as well as action-selection circuitry involving cholinergic neuromodulation responding to external cues.[83]

It is also the brain region with the highest density of α4β2 nAChR, according to Sabri's et al. *in vivo* data.[68] Functional aberrations in cholinergic signaling could therefore play an important role in shaping pathological (eating) behavior.

Rodent research showed that activation of thalamic nAChR increased the firing probability of excitatory neurons conveying auditory, sensory signals through thalamocortical pathways.[93] Interestingly, this nicotinic enhancement could be reversed by applying the high-affinity nicotinic receptor antagonist dihydro-β-erythroidine (DhβE).

One possible mechanism that underlie cholinergic importance in thalamocortical signaling could be that stimulation of thalamic nAChR induces an excitatory glutamate release onto PFC neurons, which in turn regulate processes like attention or cortical arousal.[94] Also, optical recording studies in mice showed that ACh as a neuromodulator serves to weaken intercortical circuitry and strengthens bottom-up sensory information processing through enhanced thalamocortical signaling.[95] Boswell et al.[96] compile in a meta-analysis insights from food cue reactivity research with OB study participants, summarizing similar reactivity levels comparing actual food cues with visual ones, and higher effects comparing visual to olfactory cues. Interestingly, cigarette-deprived smokers show similar thalamic fMR imaging activation patterns due to stimulation by visual smoking cues.[97] Halassa et al.[98] furthermore highlight the importance of thalamic nuclei, namely the pulvinar and the mediodorsal nucleus, in the regulation of inter- as well as intracortical functional connectivity to adapt to external stimuli, such as visual cues. Augmented thalamic gating of sensory information (through cholinergic signaling) could therefore create an attentional bias, eventually leading to overeating.

The ingestion of a high-fat diet (HFD) in mice lead to augmented levels of impulsivity and this was associated with higher prefrontal α4β2 nAChR density, as again nicotinic antagonization lead to behavior normalization.[15] Mean BMI of our OB study group was 37.8 kg/m^2 (±3.18SD), making the regular consumption of a HFD with similar long-lasting neurobiological effects for them highly probable.

Common phenomena in obesity research include higher degrees of impulsivity and loss of inhibitory control in individuals eating behavior due to alterations in several neurotransmitter signaling pathways.[11,23,99] Our data suggest that these could also be, in part, due to enhanced (cholinergic) thalamocortical signaling in OB participants compared to NW. However, this is a pilot study and data should be considered as

preliminary. Yet, findings of our study are highly relevant and should stipulate validation studies by increasing sample size.

Intra-individual V_T Assessment Between Baseline and Stimulus Conditions

The two-tailed paired samples analyses (Wilcoxon rank) investigated baseline versus stimulus α4β2 nAChR availability in NW and OB. Here, we did not find statistically significant differences in intra-individual α4β2 nAChR availability.

However, we did observe a tendency for greater V_T mean differences in OB participants compared to NW. The increase in thalamic as well as cerebellar V_T in OB between baseline and stimulus conditions was not observed in NW, where V_T remained stable. Hence, the presentation of salient food items created robust V_T differences in OB compared with NW.

As described in recent research[27,100] cholinergic signaling functions in phasic as well as tonic ACh release patterns. Phasic signaling happens in milliseconds, potentially leading to rapid neuromodulation, which is a lot faster than the temporal resolution of a PET examination can offer.[17] An interesting approach to enhance temporal resolution could be applying seed-based fMR imaging analyses to further disentangle the role of phasic signaling in the processing of sensory cues, such as food items.

Correlational Analyses of VAS Versus V_T

To investigate the relationship between cholinergic neuromodulation and eating behavior, we correlated regional α4β2 nAChR availability with VAS scores. Here, NW showed statistically significant negative correlations between different brain regions responsible for mesolimbic reward signaling (VTA and NAc), reward value attribution (OFC), interoceptive awareness (Insula) and VAS score "craving" under baseline conditions. OB demonstrated negative correlations between several brain regions relevant for reward signaling (VTA, NAc), interoceptive awareness (Insula), or cholinergic signaling (NBM, Thalamus) and VAS score "disinhibition" under baseline conditions. Less significant correlations for both study groups under stimulus conditions were found. The fact that our two study groups present different correlation profiles under baseline and stimulus conditions could highlight that altered eating behavior assessed by VAS scores can be associated with contrasting cholinergic signaling profiles.

However, the interpretation of the exact nature of our correlations is rather challenging as upregulation or desensitization of nAChR can occur[35] and this would have an impact on investigated V_T and hence correlational analyses.

We also saw differences between our study groups examining the correlation of changes in α4β2 nAChR availability and VAS Scores between baseline and stimulus conditions. While we see a significant positive correlation between HPT and "satiety" in our NW study group, a significant negative correlation between NAc and "disinhibition" in OB could be found. The first could indicate a physiological, hypothalamic energy homeostasis in NW involving cholinergic signaling.[101] The latter could once again point out to group differences in cholinergic neuromodulation influencing accumbal mesolimbic reward signaling. Paolone et al. point out that in obesity, cholinergic modulation of top down, attentional control seems to be altered in individuals who attribute high incentive salience to rewarding cues.[44] Taken together, these associations might be a further hint for disturbed hedonic pathways in obesity with reduced top-down control of mesolimbic centers towards rewarding food cues mediated by α4β2 nAChR.

Limitations

Being an exploratory analysis, we allow ourselves to look and interpret tendencies in V_T differences (p= 0.05 − 0.15) while we did not conduct a Bonferroni correction, either. Moreover, as in other neuroimaging studies number of study participants is limited and that might impact the statistical power of our analysis (n= 30 in total, baseline and stimulus examination completed n= 27). The relatively small effect size may be due to the current small sample size, as previous case number estimates indicated a participant number of at least n= 60 to achieve statistically significant group differences. The estimate was based on results (SD, mean V_T) from analogous exploratory receptor availability studies.[102,103]

It was especially challenging to recruit eligible participants with obesity due to the following reasons: they all had to be mentally healthy, non-smokers and without any neuropsychiatric medication or concomitant diseases. Yet, a lot of potential participants were suffering from mental disorders, also underlining the important association between obesity and mental disorders. Total bore size measures 60cm,

resulting in closely fitted OB examination conditions. Some potential participants even had to be ruled out due to lack of eligible body shape to fit in the scanner.

Another factor that should be discussed is the partial volume effect. One of the key regions of cholinergic signaling is the NBM. As it is a relatively small region, manually drawn VOIs of that region could therefore be vulnerable to partial volume effect errors (PVE). We used manually drawn VOIs to account for physiological alterations in individual neuroanatomy. Thomas et al. also established a toolbox to compensate for PVE in PET imaging studies, which could be a promising next step to increase neuroimaging accuracy.[104]

The calculation of primary outcome measure V_T was based on the 120-165 minutes p.i. tracer concentration in tissue (C_{tissue}) at equilibrium divided by total radioactivity concentration in venous blood plasma (C_{plasma}). Own pilot data using arterial input function without metabolite correction generated about 10% lower V_T for all regions, without important biasing effect on V_T.[68] Also, the relative standard deviation of V_T was even lower with input functions without metabolite correction. Mathematical correction for metabolization was therefore not conducted as focus of this study was the examination of baseline versus stimulus examination.

Outlook

The study is currently with extension of study participants, thus further data will be gathered to draw a specific picture of the neurobiological mechanism of cholinergic signaling in human obesity. We will also subdivide our participants in low (LD) and high disinhibition (HD) eating characteristics, according to the TFEQ[105] and investigate α4β2 nAChR availability differences between LD and HD. Next to recruitment of more study participants (N=60 in total), we will apply seed-based fMR imaging analyses to examine α4β2 nAChR availability, functional connectivity and the potential implications of these joint data analyses on neurobiological computation of salient food cues. Another next step in phase 0/I studies could include a pharmacological challenge applying partial α4β2 nAChR agonist varenicline for the examination of α4β2 nAChR occupancy and adequate dose adjustment in human clinical trials. This is in line with prior studies applying varenicline. Here, decreased sugar intake in mice[51] as well as dampened mesolimbic dopamine release in nicotine-dependent humans could be proven.[106]

Conclusion

To conclude, this study was the first in-human analysis investigating cholinergic signaling in regards to eating behavior applying specific radiotracer (-)-[^{18}F]flubatine. Our data indicate differences in α4β2 nAChR availability in OB compared to NW, especially in key regions such as the NBM and the thalamus. Specifically, higher thalamic V_T in OB can be assumed. This should lead to enhanced thalamocortical processing of sensory information and could offer a quantitative neurobiological framework for increased attentional shifts towards food cues in overweight individuals. Correlational analyses further revealed distinct group- and region-specific differences comparing VAS scores for eating behavior and α4β2 nAChR availability. Yet, due to the small sample size and heterogeneity of our study group, interpretation of these analyses requires further confirmation. If confirmed, the α4β2 nAChR represents a prospective pharmacological target for novel non-invasive treatment strategies combating the obesity epidemic.

9. Summary

Introduction: Cholinergic network modulation is carried out through the neurotransmitter acetylcholine (ACh) and expression of α4β2 nicotinic acetylcholine recetors (nAChRs) in central brain regions responsible for the detection of external sensory stimuli through thalamic and basal forebrain circuits but also within mesolimbic reward signaling. Alterations in α4β2 availability could therefore contribute to pathologically increased eating behavior leading to obesity. Investigations of task-related cholinergic neurotransmission *in vivo* in human obesity comparing baseline versus stimulus conditions have yet to be established.

Objective: Aim of this exploratory study was to investigate the neurobiological mechanisms of cholinergic signaling and its ramifications on eating behavior to possibly identify α4β2 as a pharmacological target in obesity therapy approaches. Primary outcome measure was the distribution volume calculated from PET data by VOI-based analyses. We compared α4β2 nAChR availability in OB (participants with obesity) with NW (normal weight participants) under baseline and stimulus conditions. Secondary, we explored whether changes in eating behavior measured by VAS (visual analogue scores) are correlated with changes in α4β2 nAChR availability. We also hypothesized that this relationship differs between resting state and stimulus conditions in both NW as well as OB.

Materials and Methods: Study population consisted of 16 study participants with OB (N=16; mean BMI 37.8±3.18 kg/m^2; 10 females; mean age 40.6±14.0; range from 20-62 years) and 14 NW (N=14; mean BMI 21.8±1.90 kg/m^2; 11 females; mean age 28.1±7.58; range from 19-45 years), all mentally healthy and non-smokers. Every participant underwent simultaneous PET-MR imaging (mMR Siemens) under baseline and stimulus conditions, applying a standard set of salient food items. Calculations of V_T was based on the bolus-infusion protocol. This includes investigation of V_T as the ratio between mean (-)-[^{18}F]flubatine in brain tissue and mean plasma (-)-[^{18}F]flubatine in venous blood samples at 120 until 165 minutes post injection.

During each visit VAS data were obtained.

Results: No significant group differences in V_T between NW and OB under baseline conditions were found, while OB showed a trend towards lower V_T in the Nucleus basalis of Meynert (NBM; NW: mean V_T= 11.6; OB: mean V_T=10.2; mean difference= 1.35; p= 0.119). Under stimulus conditions, OB demonstrate higher thalamic V_T (Thalamus; NW: mean V_T= 25.1; OB: mean V_T= 28.8; mean difference: -3.63; p= 0.028). Additionally, OB showed a tendency to greater V_T mean differences between resting state and stimulus conditions compared with NW. Correlational analyses revealed statistically significant positive correlation (r= 0.61) between HPT and VAS "satiety" in NW and a significant negative correlation (r= -0.59) between NAc and VAS "disinhibition" in OB.

Conclusion: These first in-human data suggest substantial changes in cholinergic signaling in brain circuits that process external sensory stimuli with high-incentive properties such as visual food cues in obesity. If confirmed in an extended population with larger sample size and including seed-based fMR imaging investigations, the α4β2 nAChR represent a promising target for pharmacological intervention as a non-invasive alternative to surgical procedures to combat the obesity epidemic.

10. References

1. Pi-Sunyer, X et al. The medical risks of obesity. *Postgrad. Med.* **121**, 21–33 (2009).

2. Piché, M. E., Tchernof, A. & Després, J. P. Obesity Phenotypes, Diabetes, and Cardiovascular Diseases. *Circ. Res.* **126**, 1477–1500 (2020).

3. Hruby, A. & Hu, F. B. The Epidemiology of Obesity: A Big Picture. *Pharmacoeconomics* **33**, 673–689 (2015).

4. Junge, K. M. *et al.* MEST mediates the impact of prenatal bisphenol A exposure on long-term body weight development. *Clin. Epigenetics* **10**, 19 (2018).

5. Arterburn, D. E. & Courcoulas, A. P. Bariatric surgery for obesity and metabolic conditions in adults. *BMJ* **349**, g3961 (2014).

6. Rupprecht, L. E., Donny, E. C. & Sveda, A. F. Obese smokers as a potential subpopulation of risk in tobacco reduction policy. *Yale J. Biol. Med.* **88**, 289–294 (2015).

7. Audrain-Mcgovern, J. & Benowitz, N. L. Cigarette Smoking, Nicotine, and Body Weight. *Clin Pharmacol Ther* **90**, 164–168 (2011).

8. Blendy, J. A. *et al.* Reduced nicotine reward in obesity: Cross-comparison in human and mouse. *Psychopharmacology (Berl).* **180**, 306–315 (2005).

9. Kovacs, M. A., Correa, J. B. & Brandon, T. H. Smoking as alternative to eating among restrained eaters: Effect of food prime on young adult female smokers. *Heal. Psychol.* **33**, 1174–1184 (2014).

10. Horstmann, A. It wasn't me; it was my brain – Obesity-associated characteristics of brain circuits governing decision-making. *Physiol. Behav.* **176**, 125–133 (2017).

11. Volkow, N. D., Wang, G. J., Tomasi, D. & Baler, R. D. Obesity and addiction: Neurobiological overlaps. *Obesity Reviews.* **14,** 2–18 (2013).

12. Mark, G. P., Shabani, S., Dobbs, L. K. & Hansen, S. T. Cholinergic modulation of mesolimbic dopamine function and reward. *Physiol. Behav.* **104**, 76–81 (2011).

13. AI, P. V. et. al. Prefrontal Ach release controls cue detection on multiple time scales. *Neuron* **56**, 141-154 (2007).

14. Locey, M. L. & Dallery, J. Nicotine and the behavioral mechanisms of intertemporal choice. *Behav. Processes* **87**, 18–24 (2011).

15. Morganstern, I., Ye, Z., Liang, S., Fagan, S. & Leibowitz, S. F. Involvement of cholinergic mechanisms in the behavioral effects of dietary fat consumption. *Brain Res.* **1470**, 24–34 (2012).

16. Sheffler, Z. M. & Pillarisetty, L. S. *Physiology, Neurotransmitters. StatPearls* (StatPearls Publishing, 2019).

17. Sander, C. Y. & Hesse, S. News and views on in-vivo imaging of neurotransmission using PET and MRI. *Q. J. Nucl. Med. Mol. Imaging* **61**, 414–428 (2017).

18. Owen, M. J., Sawa, A. & Mortensen, P. B. Schizophrenia. *Lancet (London, England)* **388**, 86–97 (2016).

19. Mc Whirter, J. J. & Kigin, T. J. Depression. *Prev. Adolesc. Suicide* **392**, 149–186 (2013).

20. H. Ferreira-Vieira, T., M. Guimaraes, I., R. Silva, F. & M. Ribeiro, F. Alzheimer's disease: Targeting the Cholinergic System. *Curr. Neuropharmacol.* **14**, 101–115 (2016).

21. Reich, S. G. & Savitt, J. M. Parkinson's Disease. *Med. Clin. North Am.* **103**, 337–350 (2019).

22. Volkow, N. D. & Morales, M. The Brain on Drugs: From Reward to Addiction. *Cell* **162**, 712–725 (2015).

23. Criscitelli, K. & Avena, N. M. The neurobiological and behavioral overlaps of nicotine and food addiction. *Prev. Med. (Baltim).* **92**, 82–89 (2016).

24. Ballinger, E. C., Ananth, M., Talmage, D. A. & Role, L. W. Basal Forebrain Cholinergic Circuits and Signaling in Cognition and Cognitive Decline. *Neuron* **91**, 1199–1218 (2016).

25. Parikh, V. & Sarter, M. Cholinergic mediation of attention: Contributions of phasic and tonic increases in prefrontal cholinergic activity. in *Annals of the New York Academy of Sciences*. **1129** 225–235 (2008).

26. Newman, E. L., Gupta, K., Climer, J. R., Monaghan, C. K. & Hasselmo, M. E. Cholinergic modulation of cognitive processing: insights drawn from computational models. *Front. Behav. Neurosci.* **6**, 1–19 (2012).

27. Sarter, M., Parikh, V. & Howe, W. M. Phasic acetylcholine release and the volume transmission hypothesis: time to move on. *Nat. Rev. Neurosci.* **10**, 383–390 (2009).

28. Graupner, M. & Gutkin, B. Modeling nicotinic neuromodulation from global

functional and network levels to nAChR based mechanisms. *Acta Pharmacol. Sin.* **30**, 681–693 (2009).

29. Zoli, M., Pucci, S., Vilella, A. & Gotti, C. Neuronal and Extraneuronal Nicotinic Acetylcholine Receptors. *Curr. Neuropharmacol.* **16**, 338–349 (2018).

30. Stojakovic, A., Espinosa, E. P., Farhad, O. T. & Lutfy, K. Effects of nicotine on homeostatic and hedonic components of food intake. *J. Endocrinol.* **235**, R13–R31 (2017).

31. A. Dani, J., Jenson, D. & I. Broussard, J. Neurophysiology of Nicotine Addiction. *J. Addict. Res. Ther.* **01**, S1 (2012).

32. Kuwabara, H. *et al.* PET Imaging of nicotinic acetylcholine receptors in baboons with 18F-AZAN, a radioligand with improved brain kinetics. *J. Nucl. Med.* **53**, 121–9 (2012).

33. Kimes, A. S. *et al.* 2-[18F]F-A-85380: PET imaging of brain nicotinic acetylcholine receptors and whole body distribution in humans. *FASEB J.* **17**, 1331–1333 (2003).

34. Changeux, J. P. Nicotine addiction and nicotinic receptors: Lessons from genetically modified mice. *Nat. Rev. Neurosci.* **11**, 389–401 (2010).

35. Marina R. Picciotto*, Nii A. Addy, Yann S. Mineur, and D. H. B. It's not "either/or": activation and desensitization of nicotinic acetylcholine receptors both contribute to behaviors related to nicotine addiction and mood. *Prog Neurobiol.* **84**, 329–342 (2008).

36. Govind, A. P., Walsh, H. & Green, W. N. Nicotine-Induced Upregulation of Native Neuronal Nicotinic Receptors Is Caused by Multiple Mechanisms. *J. Neurosci.* **32**, 2227–2238 (2012).

37. Scarr, E., Gibbons, A. S., Neo, J., Udawela, M. & Dean, B. Cholinergic connectivity: it's implications for psychiatric disorders. *Front. Cell. Neurosci.* **7**, 55 (2013).

38. Picciotto, M. R., Higley, M. J. & Mineur, Y. S. Acetylcholine as a Neuromodulator: Cholinergic Signaling Shapes Nervous System Function and Behavior. *Neuron* **76**, 116–129 (2012).

39. Picciotto, M. R. & Kenny, P. J. Molecular mechanisms underlying behaviors related to nicotine addiction. *Cold Spring Harb. Perspect. Med.* **3**, Issue 1 (2013).

40. Mansvelder, H. D., Mertz, M. & Role, L. W. Nicotinic modulation of synaptic

transmission and plasticity in cortico-limbic circuits. *Semin. Cell Dev. Biol.* **20**, 432–440 (2009).

41. Hasselmo, M. E. & Sarter, M. Modes and Models of Forebrain Cholinergic Neuromodulation of Cognition. *Neuropsychopharmacology* **36**, 52–73 (2010).

42. Y.Y. Szeto, J. & J.G. Lewis, S. Current Treatment Options for Alzheimer's Disease and Parkinson's Disease Dementia. *Current Neuropharmacology* **14,** 326-338 (2016).

43. Gritton, H. J. *et al.* Cortical cholinergic signaling controls the detection of cues. *Proc. Natl. Acad. Sci. U. S. A.* **113**, E1089-97 (2016).

44. Paolone, G., Angelakos, C. C., Meyer, P. J., Robinson, T. E. & Sarter, M. Cholinergic control over attention in rats prone to attribute incentive salience to reward cues. *J. Neurosci.* **33**, 8321–8335 (2013).

45. Hasselmo, M. E. & McGaughy, J. High acetylcholine levels set circuit dynamics for attention and encoding and low acetylcholine levels set dynamics for consolidation. *Prog. Brain Res.* **145**, 207–31 (2004).

46. Thiele, A. & Bellgrove, M. A. Neuromodulation of Attention. *Neuron* **97**, 769–785 (2018).

47. Arnsten, A. F. T. Stress signalling pathways that impair prefrontal cortex structure and function. *Nat. Rev. Neurosci.* **10**, 410–422 (2009).

48. Bloem, B., Poorthuis, R. B. & Mansvelder, H. D. Cholinergic modulation of the medial prefrontal cortex: the role of nicotinic receptors in attention and regulation of neuronal activity. *Front. Neural Circuits* **8**, 1–16 (2014).

49. Kenny, P. J. Common cellular and molecular mechanisms in obesity and drug addiction. *Nat. Rev. Neurosci.* **12**, 638–651 (2011).

50. Avena, N. M. & Rada, P. V. Cholinergic modulation of food and drug satiety and withdrawal. *Physiol. Behav.* **106**, 332–336 (2012).

51. Shariff, M. *et al.* Neuronal nicotinic acetylcholine receptor modulators reduce sugar intake. *PLoS One* **11**, (2016).

52. Avena, N. M. *et al.* After daily bingeing on a sucrose solution, food deprivation induces anxiety and accumbens dopamine/acetylcholine imbalance *Physiol Behav* **94**, 309–315 (2008).

53. Kenny, P. J., Voren, G., Johnson, P. M. & Kenny, P. Dopamine D2 receptors and striatopallidal transmission in addiction and obesity. *Curr Opin Neurobiol* **23**, 535–538 (2013).

54. Kenny, P. J. & Markou, A. Nicotine Self-Administration Acutely Activates Brain Reward Systems and Induces a Long-Lasting Increase in Reward Sensitivity. *Neuropsychopharmacology* **31**, 1203–1211 (2006).

55. Zoli, M. & Picciotto, M. R. Nicotinic regulation of energy homeostasis. *Nicotine Tob. Res.* **14**, 1270–1290 (2012).

56. Mineur, Y. S. *et al.* Nicotine Decreases Food Intake Through Activation of POMC Neurons. *Science.* **332**, 1330–1332 (2011).

57. Herman, A. M. *et al.* A cholinergic basal forebrain feeding circuit modulates appetite suppression. *Nature* **538**, (2016).

58. Kroemer, N. B., Guevara, A., Vollstädt-Klein, S. & Smolka, M. N. Nicotine Alters Food–Cue Reactivity via Networks Extending From the Hypothalamus. *Neuropsychopharmacology* **38**, 2307–2314 (2013).

59. Brust, P., van den Hoff, J. & Steinbach, J. Development of (18)F-labeled radiotracers for neuroreceptor imaging with positron emission tomography. *Neurosci. Bull.* **30**, 777–811 (2014).

60. Ichise, M., Meyer, J. H. & Yonekura, Y. An introduction to PET and SPECT neuroreceptor quantification models. *Journal of Nuclear Medicine* vol. **42**, 755-763 (2001).

61. Wong, D. F. & Gjedde, A. Monoamines: Human brain imaging. *Encycl. Neurosci.* 939–952 (2009)

62. Innis, R. B. *et al.* Consensus nomenclature for in vivo imaging of reversibly binding radioligands. *J. Cereb. Blood Flow Metab.* **27**, 1533–1539 (2007).

63. Wong, D. F. *et al.* PET imaging of high-affinity a4b2 nicotinic acetylcholine receptors in humans with 18F-AZAN, a radioligand with optimal brain kinetics. *J. Nucl. Med.* **54**, 1308–1314 (2013).

64. Hillmer, A. T. *et al.* PET Imaging of 4 2* Nicotinic Acetylcholine Receptors: Quantitative Analysis of 18F-Nifene Kinetics in the Nonhuman Primate. *J. Nucl. Med.* **53**, 1471–1480 (2012).

65. Horti, A. G., Kuwabara, H., Holt, D. P., Dannals, R. F. & Wong, D. F. Recent PET radioligands with optimal brain kinetics for imaging nicotinic acetylcholine receptors. *J. Label. Compd. Radiopharm.* **56**, 159–166 (2013).

66. Brody, A. L. *et al.* Cigarette Smoking Saturates Brain α 4 β 2 Nicotinic Acetylcholine Receptors Angeles; Greater Los Angeles Veterans Affairs Healthcare System Positron Emission Tomography Center (. *Arch Gen*

Psychiatry **63**, 907–915 (2006).

67. Mukhin, Alexey; Iane S. Kimes1, Svetlana I. Chefer1, John A. Matochik1, Carlo S. Contoreggi2, Andrew G. Horti3, D. Bruce Vaupel1, Olga Pavlova1, and E. A. S. Greater Nicotinic Acetylcholine Receptor Density in Smokers Than in Nonsmokers: A PET Study with 2-18 F-FA-85380. *PLoS One* **32**, 736–740 (2017).

68. Sabri, O. *et al.* First-in-human PET quantification study of cerebral α4β2* nicotinic acetylcholine receptors using the novel specific radioligand (-)-[18F]Flubatine. *Neuroimage* **118**, 199–208 (2015).

69. Patt, M. *et al.* Evaluation of metabolism, plasma protein binding and other biological parameters after administration of (-)-[18F]Flubatine in humans. *Nucl. Med. Biol.* **41**, 489–494 (2014).

70. Tiepolt, S. *et al.* (+)-[18F]Flubatine as a novel α4β2 nicotinic acetylcholine receptor PET ligand—results of the first-in-human brain imaging application in patients with β-amyloid PET-confirmed Alzheimer's disease and healthy controls. *Eur. J. Nucl. Med. Mol. Imaging* **48**, 731–746 (2021).

71. Hockley, B. G. *et al.* (-)-[18F]Flubatine: Evaluation in rhesus monkeys and a report of the first fully automated radiosynthesis validated for clinical use. *J. Label. Compd. Radiopharm.* **56**, 595–599 (2013).

72. Gallezot, J.-D. *et al.* Evaluation of the sensitivity of the novel α4β2* nicotinic acetylcholine receptor PET radioligand 18F-(-)-NCFHEB to increases in synaptic acetylcholine levels in rhesus monkeys. *Synapse* **68**, 556–64 (2014).

73. Ding, Y. S. *et al.* Dopamine receptor-mediated regulation of striatal cholinergic activity: Positron emission tomography studies with norchloro [18F] fluoroepibatidine. *J. Neurochem.* **74**, 1514–1521 (2000).

74. Esterlis, I. *et al.* Imaging changes in synaptic acetylcholine availability in living human subjects. *J. Nucl. Med.* **54**, 78–82 (2013).

75. Hillmer, A. T. *et al.* Imaging of cerebral α4β2* nicotinic acetylcholine receptors with (-)-[(18)F]Flubatine PET: Implementation of bolus plus constant infusion and sensitivity to acetylcholine in human brain. *Neuroimage* **141**, 71–80 (2016).

76. Hillmer, A. T. & Carson, R. E. Quantification of PET infusion studies without true equilibrium: A tissue clearance correction. *J. Cereb. Blood Flow Metab.* **40**, 860–874 (2020).

77. Shan, B., Chai, P. & Zhang, Z. Positron emission tomography. *Advanced*

Topics in Science and Technology in China, 214-312 (2013).

78. Rasia-Filho, A. A., Londero, R. G. & Achaval, M. Functional activities of the amygdala: An overview. *Journal of Psychiatry and Neuroscience* **25**, 14-23 (2000).

79. Grahn, J. A., Parkinson, J. A. & Owen, A. M. The cognitive functions of the caudate nucleus. *Prog. Neurobiol.* **86**, 141–55 (2008).

80. Menon, V., Uddin, L. Q., Struct, B. & Author, F. Saliency, switching, attention and control: a network model of insula function. *Brain Struct Funct* **214**, 655–667 (2010).

81. E. Rolls et al. The orbitofrontal cortex. *Philos. Trans. R. Soc. London. Ser. B Biol. Sci.* **351**, 1433–1444 (1996).

82. Buchsbaum, M. S. Frontal Cortex Function. *Am. J. Psychiatry* **161**, 2178–2178 (2004).

83. Ding, J. B., Guzman, J. N., Peterson, J. D., Goldberg, J. A. & Surmeier, D. J. Thalamic gating of corticostriatal signaling by cholinergic interneurons. *Neuron* **67**, 294–307 (2010).

84. Bryant, E. J., Rehman, J., Pepper, L. B. & Walters, E. R. Obesity and Eating Disturbance: the Role of TFEQ Restraint and Disinhibition. *Curr. Obes. Rep.* **8**, 363–372 (2019).

85. Westenhoefer, J., Broeckmann, P., Münch, A. K. & Pudel, V. Cognitive control of eating behavior and the disinhibition effect. *Appetite.* **23,** 27–41 (1994).

86. Patt, M. *et al.* Fully automated radiosynthesis of both enantiomers of [18F]Flubatine under GMP conditions for human application. *Appl. Radiat. Isot.* **80**, 7–11 (2013).

87. Schütz, L. *et al.* Feasibility and acceptance of simultaneous amyloid PET/MRI. *Eur. J. Nucl. Med. Mol. Imaging* **43**, 2236–2243 (2016).

88. Catana, C. *et al.* Toward implementing an MRI-based PET attenuation-correction method for neurologic studies on the MR-PET brain prototype. *J. Nucl. Med.* **51**, 1431–8 (2010).

89. Bentley, P., Driver, J. & Dolan, R. J. Cholinergic modulation of cognition: Insights from human pharmacological functional neuroimaging. *Prog. Neurobiol.* **94**, 360–388 (2011).

90. Mair, R. G., Onos, K. D. & Hembrook, J. R. Cognitive activation by central thalamic stimulation: The yerkes-dodson law revisited. *Dose-Response* **9**, 313–

331 (2011).

91. Quick, M. W. & Lester, R. A. J. Desensitization of neuronal nicotinic receptors. *J. Neurobiol.* **53**, 457–478 (2002).

92. Dezfuli, G. *et al.* Evidence for the role of β2* nAChR desensitization in regulating body weight in obese mice. *Neuropharmacology* **110**, 165–174 (2016).

93. Kawai, H., Lazar, R. & Metherate, R. Nicotinic control of axon excitability regulates thalamocortical transmission. *Nat. Neurosci.* **10**, 1168–1175 (2007).

94. Lambe, E. K., Picciotto, M. R. & Aghajanian, G. K. Nicotine induces glutamate release from thalamocortical terminals in prefrontal cortex. *Neuropsychopharmacology* **28**, 216–225 (2003).

95. Kimura, F. Acetylcholine suppresses the spread of excitation in the visual cortex revealed by optical recording: Possible differential effect depending on the source of input. *Eur. J. Neurosci.* **11**, 3597–3609 (1999).

96. Boswell, R. G. & Kober, H. Food cue reactivity and craving predict eating and weight gain: A meta-analytic review. *Obes. Rev.* **17**, 159–177 (2016).

97. Due, D. L., Huettel, S. A., Hall, W. G. & Rubin, D. C. Activation in mesolimbic and visuospatial neural circuits elicited by smoking cues: Evidence from functional magnetic resonance imaging. *Am. J. Psychiatry* **159**, 954–960 (2002).

98. Halassa, M. M. & Kastner, S. Thalamic functions in distributed cognitive control. *Nat. Neurosci.* **20**, 1669–1679 (2017).

99. Wang, G. J. *et al.* Brain dopamine and obesity. *Lancet* **357**, 354–357 (2001).

100. Sarter, M. *et al.* What do phasic cholinergic signals do? *Neurobiol. Learn. Mem.* **130**, 135–141 (2016).

101. Calarco, C. A. & Picciotto, M. R. Nicotinic Acetylcholine Receptor Signaling in the Hypothalamus: Mechanisms Related to Nicotine's Effects on Food Intake. *Nicotine and Tobacco Research.* **22**, 152–163 (2020).

102. Dupont, W. D. & Plummer, W. D. Power and sample size calculations. A review and computer program. *Control. Clin. Trials* **11**, 116–128 (1990).

103. Hesse, S. *et al.* The serotonin transporter availability in untreated early-onset and late-onset patients with obsessive-compulsive disorder. *Int. J. Neuropsychopharmacol.* **14**, 606–617 (2011).

104. Thomas, B. A. *et al.* PETPVC: A toolbox for performing partial volume

correction techniques in positron emission tomography. *Phys. Med. Biol.* **61**, 7975–7993 (2016).

105. Stunkard, A. J. & Messick, S. The three-factor eating questionnaire to measure dietary restraint, disinhibition and hunger. *J. Psychosom. Res.* **29**, 71–83 (1985).

106. McCaul, M. E. *et al.* The Relationship of Varenicline Agonism of α4β2 Nicotinic Acetylcholine Receptors and Nicotine-Induced Dopamine Release in Nicotine-Dependent Humans. *Nicotine Tob. Res.* **22**, 892–899 (2020).

11. Anlagen

Funding